International Journal of Solids and Structures 283 (2023) 112487

Contents lists available at ScienceDirect

International Journal of Solids and Structures

journal homepage: www.elsevier.com/locate/ijsolstr

The work input to saturated porous media undergoing internal erosion

Dat G. Phan [a], Giang D. Nguyen [a,*], Ha H. Bui [b]

[a] School of Architecture and Civil Engineering, The University of Adelaide, Adelaide SA 5005, Australia
[b] Department of Civil Engineering, Monash University, Clayton, Victoria 3800, Australia

ARTICLE INFO

Keywords:
Internal erosion
Porous media
Effective stress
Thermodynamics
Constitutive modelling
Hydro-mechanical coupling

ABSTRACT

The mechanism of internal erosion in porous media involves the microstructural evolutions induced by washing out of fine particles under different loading and seepage flow actions. Consequently, the effective stress on the solid skeleton is governed by the transition in velocity and stress of fine particles due to their detachment from the skeleton and then transport through pore channels, in addition to pore pressure. This study is to develop a formulation of work input to account for the interactions and mass exchanges between solid and fluid phases. Coupled mechanical-hydraulic erosion processes can be properly reflected through mass, momentum and energy balances based on Biot's mixture theory of a three-phase model. This leads to three separate stress-like variables, effective stress, erosion force and hydraulic gradient, in conjugation with three strain-like variables, strain, mass loss and seepage velocity, respectively. The effective stress tensor, different from the classical form by Terzaghi due to the effect of erosion, and coupled hydro-mechanical-erosion criteria are naturally derived from the proposed work input. They consider grain scale mechanisms describing the transition of erodible particles from the solid skeleton to the fluidized state. Systematic formulations and discussions are presented to highlight the promising features of our approach.

1. Introduction

Internal erosion has been frequently encountered in many geo-hazards (e.g. failure of embankment, sinkholes and cavities in dams and dikes) (Foster et al., 2000). This phenomenon involves the volume change and progressive degradation of soil strength due to the mass loss triggered by hydrodynamic forces of fluid flows as observed in several experiments (Kuwano et al., 2021; Liang et al., 2019; Prasomsri and Takahashi, 2020; Sato and Kuwano, 2018). It is governed by the mutual solid-fluid transformations and interactions (Hu et al., 2019; Zhou et al., 2020) under inseparable effects of several key factors: soil susceptibility (Chang and Zhang, 2013; Wan and Fell, 2008), stress condition (Bendahmane et al., 2008; Chang and Zhang, 2011), and hydraulic gradient (Moffat and Fannin, 2006).

The macro hydromechanical behaviour of fully saturated porous media under the effects of internal erosion is intrinsically linked to the grain-scale interaction between the movement of eroded grains and seepage flow. This interaction has been extensively investigated in numerous experiments (Chang and Zhang, 2013; Hunter and Bowman, 2018; Prasomsri and Takahashi, 2020; Sato and Kuwano, 2018; Nguyen et al., 2018; Nguyen et al., 2019) and numerical studies using the coupled hydro-mechanical numerical methods (e.g. DEM-CFD) for insights into grain scale mechanisms (Cheng et al., 2021; Gu et al., 2019; Hu et al., 2020; Yin et al., 2021; Zou et al., 2020). It is reflected through continuous actions of detachment of erodible particles from the soil skeleton and followed by their transport through pore channels (Zhou et al., 2020; Bonelli and Marot, 2011) in various loading and seepage flow conditions. This transition usually exhibits sudden changes of velocity and stress on erodible fine particles within a short timeframe, associated with the release of strain energy due to loss of grain-to-grain contacts (Liu et al., 2020). As a consequence, the lateral support of fine particles in the force chain of the soil skeleton is suddenly lost (Liu et al. 2020; Hu et al., 2019), causing the variation in the averaged effective stress at the macro scale. This change of effective stress due to erosion should be taken into account in constitutive modelling of soils considering erosion effects.

Given the above physical observations, the grain scale mechanisms of internal erosion should be essentially reflected by the representative macroscopic variables and their evolutions from the aspects of constitutive modelling. For example, in some models (Wang et al., 2020; Zhang et al., 2015; Muir Wood et al, 2010), the evolution of additional erosion variables is used to track effects of mass losses on the stress-strain behaviour. Nevertheless, an erosion criterion that is usually a

* Corresponding author.
E-mail address: giang.nguyen@trinity.oxon.org (G.D. Nguyen).

https://doi.org/10.1016/j.ijsolstr.2023.112487
Received 26 May 2023; Received in revised form 29 August 2023; Accepted 11 September 2023
Available online 12 September 2023

Nomenclature

x_j	the spatial coordinate
t	the current time
V	the current volume
V^s	the partial volume of the solid phase
V^{es}	the partial volume of the transition phase
V^{wf}	the partial volume of the mixture of water-fluidized flow
S	the surface area S of volume V
n_j	the outward unit normal vector on the surface S
n^s	the volume fraction of the solid phase
n^{es}	the volume fraction of the transition phase
n^{wf}	the volume fraction of the mixture of water-fluidized flow
n^w	the volume fraction of the water phase
ρ	the average mass density of the mixture
$\overline{\rho}^s$	the partial mass density of the solid phase
$\overline{\rho}^{es}$	the partial mass density of the transition phase
$\overline{\rho}^{wf}$	the partial mass density of the mixture of water-fluidized flow
ρ^s	the intrinsic density of the solid phase
ρ^{es}	the intrinsic density of the transition phase
ρ^{wf}	the intrinsic density of the mixture of water-fluidized flow
ρ^w	the intrinsic density of the water phase
σ_{ij}	the total stress tensor
$\sigma_{ij}^{'}$	the effective stress tensor
$\overline{\sigma}_{ij}^s$	the partial stress of the solid phase
$\overline{\sigma}_{ij}^{es}$	the partial stress of the transition phase
$\overline{\sigma}_{ij}^{wf}$	the partial stress of the mixture of water-fluidized flow
σ_{ij}^s	the intrinsic stress tensor of the solid phase
σ_{ij}^{es}	the intrinsic stress tensor of the transition phase
σ_{ij}^{wf}	the intrinsic stress tensor of the mixture of water-fluidized flow
p	the total mean stress
p^s	the mean intrinsic stress of the solid phase
p^w	the water pressure
p^{es}	the mean intrinsic stress of the transition phase
$p^{'}$	the effective mean stress
q	the deviatoric stress
$\overline{p}$	the Terzaghi mean stress
δ_{ij}	the Kronecker delta
ρ_{ex}^{s-es}	the mass exchanges between solid and transition phases
ρ_{ex}^{es-f}	the mass exchanges between transition and fluidized phases
ρ_{ex}	the mass exchange
v_i^s	the velocity of solid phase
v_i^{es}	the velocity of transition phase
v_i^w	the water velocity
B_i	the body force of the mass $\overline{\rho}^{\varkappa} dV$ induced by the gravity acceleration constant g
R_i^s	the viscous drag force acting on the solid phase
R_i^{es}	the viscous drag force acting on the transition phase
R_i^{wf}	the viscous drag force acting on the mixture of water-fluidized flow
R_i^f	the viscous drag force acting on the fluidized phase
R_i^w	the viscous drag force acting on the water phase
L	the power input
ε_{ij}	the strain tensor
α, β	parameters controlling transition between solid and fluid-like phases of erodible particles during erosion processes
$p_e^{'}$	the erosion-driving force
θ_i	the water flux
ε_v	the volumetric strain
ε_s	the deviatoric strain
E	the erosion index
ρ_{ex}^u	the ultimate mass loss
ψ	the Helmholtz free energy
μ	the function of E used for describing the effect of erosion on the elastic stiffness
$\widetilde{\Phi}$	the dissipation potential
$\overline{\chi}^v$	the thermodynamic conjugates to rates of volumetric plastic strain $\dot{\varepsilon}_v^{\mathrm{p}}$
$\overline{\chi}^s$	the thermodynamic conjugates to rates of deviatoric plastic strain $\dot{\varepsilon}_s^{\mathrm{p}}$
$\overline{\chi}^e$	the thermodynamic conjugates to rates of erosion index $\dot{E}$
$\overline{\chi}^w$	the thermodynamic conjugates to rates of water flux θ_i
χ^v	the volumetric dissipative generalised stress
χ^s	the deviatoric dissipative generalised stress
χ^e	the erosion dissipative generalised stress
χ_i^w	the hydraulic dissipative generalised stress
$\widetilde{\Phi}^{\mathrm{me}}$	the mechanical dissipation potential
$\widetilde{\Phi}^{\mathrm{h}}$	the hydraulic dissipation potential
z^w	the rate-dependent potential
φ^v, φ^s, φ^e	functions of stresses, internal variables (plastic strain and E) and hydraulic gradient $\frac{\partial p^w}{\partial x_i}$
φ_i^w	the function dependent on θ_i to reflect rate-dependent hydraulic dissipation
C	the kinematic constraint
A, B	the general functions governing dilation responses
Λ	the Lagrangian kinematic multiplier
$y^{*(m)}$	the mechanical yield function in generalised stress space (χ_v, χ_s)
$y^{*(e)}$	the erosion criterion in generalised dissipative stress space of χ^e
$\dot{\lambda}_m$	the plasticity multiplier
$\dot{\lambda}_e$	the erosion multiplier
Π, Λ, Ω, Υ	terms in the tangent stiffness matrix
D^{vv}, D^{vs}, D^{ve}, D^{sv}, D^{ss}, D^{se}, D^{ev}, D^{es}, D^{ee}	terms of the tangent stiffnes written in the form of effective stress ($p^{'}$, q).
ϕ	the function of n^s, n^{es}, n^{wf}

result of experimental investigations (Wan and Fell, 2004; Zhou et al., 2019; Cividini et al, 2009), based on relationships between hydraulic gradients and fine content or mass loss, is missing in these models. As a consequence, the ability to capture the influences of onset and evolution of erosion processes on the response of soils is not adequate in the above-mentioned models, due to lacking terms for representing the behaviour of fluid phase (e.g. hydraulic gradient, seepage velocity) and the hydromechanical coupling. In other words, the interdependence between seepage flow and transport of eroded grains is not reflected well in these models. The coupled hydro-mechanical-erosion response has been well recognised in Yang et al. (2019) where an erosion law representing the relationship between hydraulic gradient and mass loss is adopted. This erosion law considers an essential critical threshold of hydraulic shear stress at which the internal erosion starts to take place (Wan and Fell, 2004; Zhou et al., 2019; Cividini et al, 2009). However, this study (Yang et al., 2019) neglected the effects of mass exchange and interaction between phases (solid, water) during erosion. Therefore the identification of variables used in erosion law can be questionable, affecting the

predictive capability of the model in reproducing the macro behaviour governed by the grain-scale mechanisms of the transition from contactable to floating states of eroded grains.

Numerical studies (e.g. using DEM-CFD) have shown the change of contact forces as a consequence of the loss of fine grains that carry non-neglectable levels of energy (and hence stress). This loss of contact forces due to erosion induces a change in effective stress, which should be reflected in a thermodynamic framework for continuum modelling. In this sense, better descriptions of the coupled hydro-mechanical behaviour in internal erosion, accounting for the interaction between states of eroded grains from being attached to the solid skeleton to fluidized, has successfully been addressed in several studies (Steeb and Diebels, 2003; Rousseau et al., 2020; Zhang et al., 2013). These studies use thermodynamics-based approaches to incorporate rigorously and systematically all essential behavioural characteristics associated with internal erosion in constitutive models. In these models, appropriate forms of work input are derived using fundamental mass balance and momentum equations and energy principles to identify work conjugated variables representing mutually coupled processes of seepage, particle transport, and mechanical response. As a result, they are able to capture the coexisting mechanical and hydraulic terms for reflecting the interactions between the mechanical deformation and seepage flow dependent on the mass exchange. Nevertheless, the sudden transitions in stress and velocity of eroded grains from solid to fluidized states as observed in grain scale simulations by Liu et al. (2020) and Zhou et al. (2020) are not reflected well in these studies, resulting in lack of effect of erosion on effective stress of the soil skeleton.

This paper provides a formulation of work input to describe the effects of grain-scale mechanisms of internal erosion on the effective stress and behaviour of a continuum model. Our proposed form of work input accounts for the interaction between volume change, mass loss and seepage flow along with the sudden transition in different stress and velocity regimes of erodible particles during erosion. A thermodynamics-based approach taking into account the transitions of fine particles from soil skeleton to fluidized state is adopted in this study. Using Biot's mixture theory, fully saturated porous media are made up of three constituents representing three phases of the solid-fluid mixture (e.g. soil skeleton, transition, fluidization) during erosion, where each of them is assumed to be continuous and occupies every material point in the space at any arbitrary time instant. The transition phase is needed to describe the sudden change in stress and velocity of erodible particles during erosion within a very short time. The obtained formulation of work input can capture the inseparable interaction between solid and fluid states and phases through three work conjugate variable pairs (e.g. effective stress-strain, seepage force-water flux and erosion force-mass loss). This allows us to naturally derive appropriate forms of the effective stress contributed by each phase and its volume fraction, implying its dependence on the material geometry properties and the transition process. A generic coupled hydro-mechanical model, including plasticity, seepage, erosion criteria and their interactions can also be formulated from the proposed work input and effective stress using a thermodynamics-based approach.

The outline of this paper is as follows. In Section 2, micromechanical observations as the basis for continuum modelling are analysed, followed by corresponding assumptions and basic principles of Biot's mixture theory. The formulation of the work input to saturated soils undergoing internal erosion is presented in Section 3. Details on how to use the obtained theoretical findings for the development of a generic constitutive model are presented in Section 4, followed by the conclusion in Section 5.

2. Micromechanical basis and assumptions for continuum modelling

Essential micromechanical basis and basic concepts of Biot's mixture theory (Biot, 1941; Zienkiewicz et al., 1990) for internal erosion of fully saturated porous media are introduced in this section.

2.1. Micromechanical basis

The overall response of eroded soils is dependent on the state of the solid skeleton, how the solid-water phases are connected and transformed, and the way forces interact along these interfaces at the grain scale. From the aspects of constitutive modelling, the material behaviour at the grain scale can be represented by the representative macroscopic variables (Yang et al., 2015; Vernerey, 2011) and their evolutions during erosion processes. Direct one-to-one mapping is usually impossible given a huge amount of grain scale information against a few internal variables of the constitutive model representing grain scale processes. Therefore, key grain scale mechanisms should be understood and encapsulated in a few macro quantities of a constitutive model.

Given the numerical results on the evolution of the average ratio between contact and fluid forces on the fine particles (e.g. Particles 1, 2 and 3, see Fig. 1) based on DEM-CFD (Liu et al., 2020), it can be observed that the decrease in the contact forces in eroded particles (and increase in their velocities) takes place suddenly. They undergo a transition between a state where they remain within the strong contact networks and a state where they detach from the soil skeleton and transport freely as fluid flows. The whole amount of these grains is not eroded at once because different groups of particles undergo this transition process at different times. In other words, if a few groups of several particles are fully eroded over a large enough time scale, at a given instant within that time scale, only a fraction of these particles is fully eroded. Clogging can also happen and result in particles trapped in the pores that could contribute to the stress transfer mechanisms in the soil skeleton. The net effect of erosion and clogging is assumed to be erosion-dominated. Collective (or homogenised) behaviour of all groups of particles undergoing erosion and clogging over a time scale suitable for continuum modelling results in a distinct phase that has velocity and stress between their corresponding fluid and solid counterparts. This intermediate phase is termed transition phase in this study, reflecting the fast or slow transition from solid to fluid. It is noted that the existence of this phase is associated with continuum constitutive modelling, to reflect effects of erosion and clogging over a continuum time scale.

This transition phase reflects the underlying erosion process, together with the interactions between solid and fluidised phases over a large enough time scale appropriate for continuum constitutive modelling. These interactions are totally missing in existing approaches, leading to no influence of erosion on effective stress in existing studies,

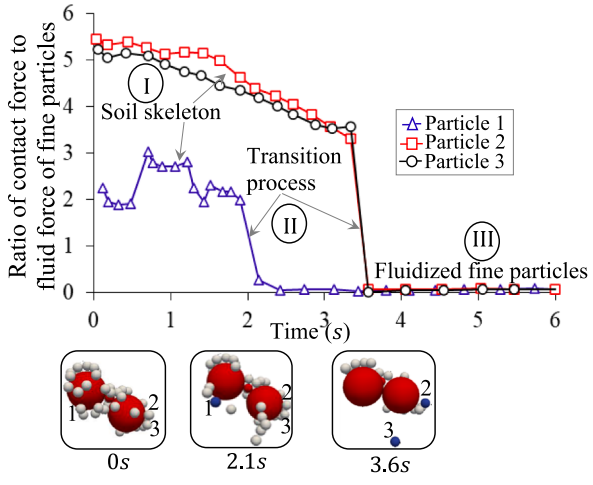

Fig. 1. Evolution of the ratio of the average contact force to the fluid force for the fine particles in a local packing (results, after Liu et al. (2020), are replotted in the figure).

which is not appropriate in our opinions.

The mechanism of internal erosion of erodible particles can be, thus, described through three continuous states (see Fig. 1):

(I) Solid-like state: staying within strong contact networks of the soil skeleton (e.g. including both fine and coarse particles) and carrying physical properties of soil skeleton,
(II) Transition state: stress-drop in weak contact networks before detaching from the soil skeleton in higher velocities and
(III) Fluidized state: free transport within voids as fluid flows.

These states are intrinsically associated with the release of kinematic strain energy stored in contacts produced by the transmission of velocity and force/stress (see Fig. 1) on erodible particles during their transition from contactable to floating (e.g. fluid-like) states. The detachment of fine particles from the soil skeleton, induced by the fluid flow, weakens the soil skeleton since fine particles connect the stress-transfer matrix. As a result, the contact force chains are suddenly buckled with a local burst of kinetic energy, leading to a sudden rearrangement of particles into a new equilibrium and then a decrease in inter-particle voids. It induces a change in volume and effective stress at the macro level. Such microscopic mechanisms are of importance to understanding the effects of internal erosion on the soil response.

The above-metioned features will be used in this study to identify a micromechanical basis and corresponding assumptions for our thermodynamics-based continuum framework. In particular, the transition from solid to fluidised observed from the above micromechanical analysis (Liu et al., 2020) can be generalised, using several groups of

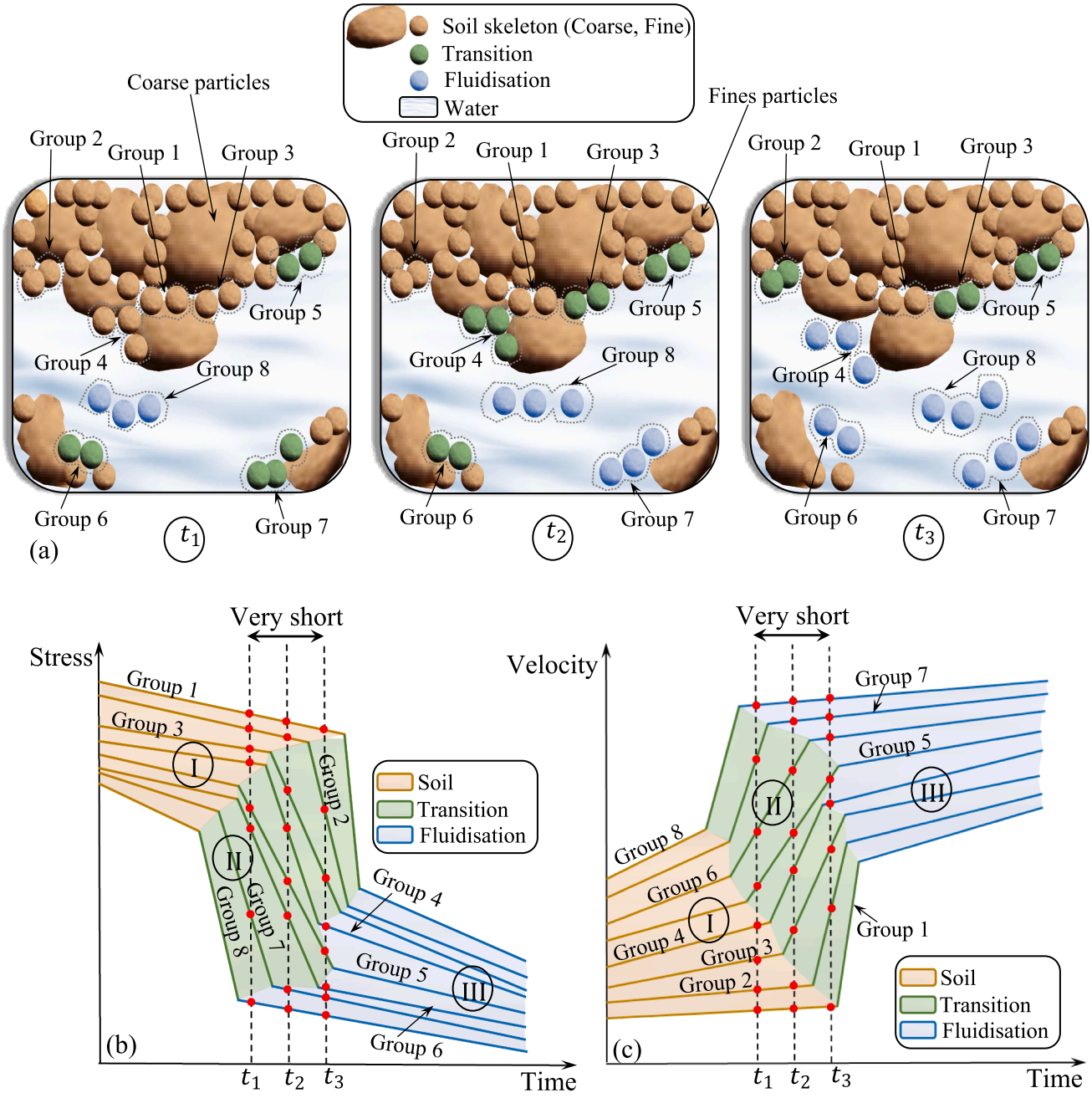

Fig. 2. Illustration on the transition mechanism of eight groups of fine particles during erosion (a) Configuration of particles within fully saturated soils (b) Evolution in stress (c) Evolution in velocity.

particles, each of which is associated with a different time of transition. In this presentation, eight typical groups of fine particles, representing eight possible erosion cases within a short timeframe, from t_1, to t_2 and t_3 (Fig. 2), can be assumed and presented in Fig. 2. Each group includes several fine particles at the same state of transformation from solid to fluidised. As seen in the micromechanical analysis of results obtained from Liu et al. (2020) (see Fig. 1), this transition can be reasonably assumed to happen within a very short time from t_1 to t_3. For continuum modelling, it is also assumed that the state of all particles in each group are a result of both erosion and deposition within a short timeframe from t_1 to t_3. In other words, net effect of both erosion and deposition results in the state of all particles in each group.

Based on Fig. 1, properties of each group can be described through assumptions of their evolutions in stress (decrease) (see Fig. 2b) and velocity (increase) (see Fig. 2c) between three regimes: (I) soil skeleton, (II) transition and (III) fluidisation, as summarised in Table 1.

It can be seen in Fig. 2 and Table 1 that there are always three states of fine particles (still attached to soil skeleton, in transition state, fully fluidised) coexisting within an eroding soil specimen at a given instant (e.g. t_1, or t_2 or t_3), apart from coarse particles and fluid. Therefore within a time scale appropriate for continuum modelling, at a given instant a transition phase for fine particles in-between the states of fluid and solid (skeleton) must exist. Given this mechanim, a three-phase-framework under isothermal condition can be assumed based on the evolution of erosion processes described above and in Fig. 2. The three phases, depecited in Fig. 3, are:

(i) solid phase with both coarse and fine particles in strong contact networks, considered as the soil skeleton (denoted as "*s*");
(ii) transition phase consisting of fine particles that are still in the transition from solid to fluidised. This phase transition from the soil-skeleton to the fluidized-particle constituents is associated with mass production, velocity and stress variation of fine particles in weak contact networks (denoted as "*es*");
(iii) water-fluidized phase is a mixture of fluid and mobilized solid particles in water (fluidised) (denoted as "*wf*", a combination of "*w*" of the original water phase and "*f*" of the fluidised phase).

We note that these above phases represent both original (e.g. solid, water) and production phases (e.g. transition, fluidised fines) linked through the mass exchanges ($\dot{\rho}_{ex}^{s-es}$ representing the mass exchange between "*s*" and "*es*" phases, $\dot{\rho}_{ex}^{es-f}$ representing the mass exchange between "*es*" and "*f*" phases) during the erosion process. They involve the transition in velocity and intrinsic stress, as shown in Figs. 1 and 2.

In this framework, the solid velocity v_i^s, intrinsic solid stress σ_{ij}^s and intrinsic density of solid ρ^s are used for the solid phase. The response of the water-fluidized flow phase (e.g. including fluidized and water phases) is characterised by the water velocity v_i^w, the intrinsic water pressure $\sigma_{ij}^{wf} = p^w \delta_{ij}$ (p^w being water pressure, δ_{ij} being Kronecker delta) and the intrinsic density of the water-fluidized phase ρ^{wf} being the combination of intrinsic solid and water densities (see further details in Section 2.2). The transition phase owns intrinsic solid density ρ^s, while its velocity v_i^{es} and intrinsic stress σ_{ij}^{es} can be averaged values of solid and water phases and can be further discussed later in Section 3.1. It can be addressed that the proposed transition phase is not considered in all existing studies on erosion despite its existence (at continuum scale) and importance for understanding the intrinsic mechanisms of internal erosion. This is the key difference from other existing theoretical studies on internal erosion.

It is acknowledged that these assumptions may be still far from perfection, given the use of an approach that requires several phenomenological treatments based on CFD-DEM modelling in the context of lacking strong experimental data. Our paper is a step towards better understanding the mechanism of internal erosion in fully saturated soils, and further investigation is still required in future work.

Table 1
Summary of states of eight fine-particle groups at t_1, t_2 and t_3.

	t_1	t_2	t_3
Group (1)	Solid	Solid	Solid
Group (2)	Solid	Solid	Transition
Group (3)	Solid	Transition	Transition
Group (4)	Solid	Transition	Fluidisation
Group (5)	Transition	Transition	Transition
Group (6)	Transition	Transition	Fluidisation
Group (7)	Transition	Fluidisation	Fluidisation
Group (8)	Fluidisation	Fluidisation	Fluidisation

2.2. Basic principles and concepts for continuum modelling

In Biot's mixture theory, definitions of volume fraction are fundamental for the development of any framework of porous media. They are the results of mathematical integration and average techniques of microscopic quantity over volume and area of a Representative Volume Element (REV) to obtain the averaged macroscopic quantities (Gray et al., 2009; Loret and Rizzi, 1999; Ricken et al., 2022). As illustrated in Fig. 2, their basis is the current total volume V (superimposed continua) defined as the sum of the partial volumes $V^\varkappa$:

$$V = V^s + V^{es} + V^{wf} \tag{1}$$

where the superscript $\varkappa$ denotes the constituent with "$\varkappa$" standing for "*s*" for soil skeleton, or "*es*" for the transition phase, or "*wf*" for the mixture of water-fluidized flow.

The volume fraction $n^\varkappa$ can be expressed as a variable related to the current volume V based on Eq. (1), taking the following form:

$$n^\varkappa = \frac{V^\varkappa}{V} \tag{2}$$

It is noted that $n^\varkappa$ are Eulerian volume fractions, which are different from Lagrangian porosities related to the initial overall porous volume, as mentioned in Coussy et al., (2010), Gajo (2011) and Sciarra (2016).

The volume fraction of each phase $n^\varkappa$ of the media meets the following condition of mixture theory:

$$n^s + n^{es} + n^{wf} = 1 \tag{3}$$

Given volume fractions written in Eq. (2), we can write the average mass density of the mixture ρ as:

$$\rho = \overline{\rho}^s + \overline{\rho}^{es} + \overline{\rho}^{wf} = n^s\rho^s + n^{es}\rho^s + n^{wf}\rho^{wf} = n^s\rho^s + n^{es}\rho^s + n^f\rho^s + n^w\rho^w \tag{4}$$

where $\overline{\rho}^\varkappa = n^\varkappa\rho^\varkappa$ is the partial mass density with $\rho^\varkappa$ being the intrinsic density of phase $\varkappa$. The intrinsic density of the water-fluidized phase is assumed to be $\rho^{wf} = \frac{n^f\rho^s + n^w\rho^w}{n^f + n^w} = \frac{n^f\rho^s + n^w\rho^w}{n^{wf}}$ to reflect the mixture between phases of original water and eroded/fluidized particles. The assumption of incompressibility of each constituent is employed with constant intrinsic densities (Madeo, et al., 2013).

Using Biot's mixture theory allows us to write the total stress tensor σ_{ij} of the whole system as a combination of partial stresses $\overline{\sigma}_{ij}^\varkappa = n^\varkappa\sigma_{ij}^\varkappa$:

$$\sigma_{ij} = \overline{\sigma}_{ij}^s + \overline{\sigma}_{ij}^{es} + \overline{\sigma}_{ij}^{wf} = n^s\sigma_{ij}^s + n^{es}\sigma_{ij}^{es} + n^{wf}p^w\delta_{ij} \tag{5}$$

with $\sigma_{ij}^\varkappa$ being the intrinsic stress tensor of phase $\varkappa$.

3. Formulation

Given the assumptions and basic principles in Section 2, this section presents a systematic procedure for deriving the formulation of work input for fully saturated soils under the effects of internal erosion. The approach for the derivation of work input (Houlsby, 1979; Houlsby, 1997, Einav and Liu, 2018) is used as the basis for saturated soils undergoing internal erosion.

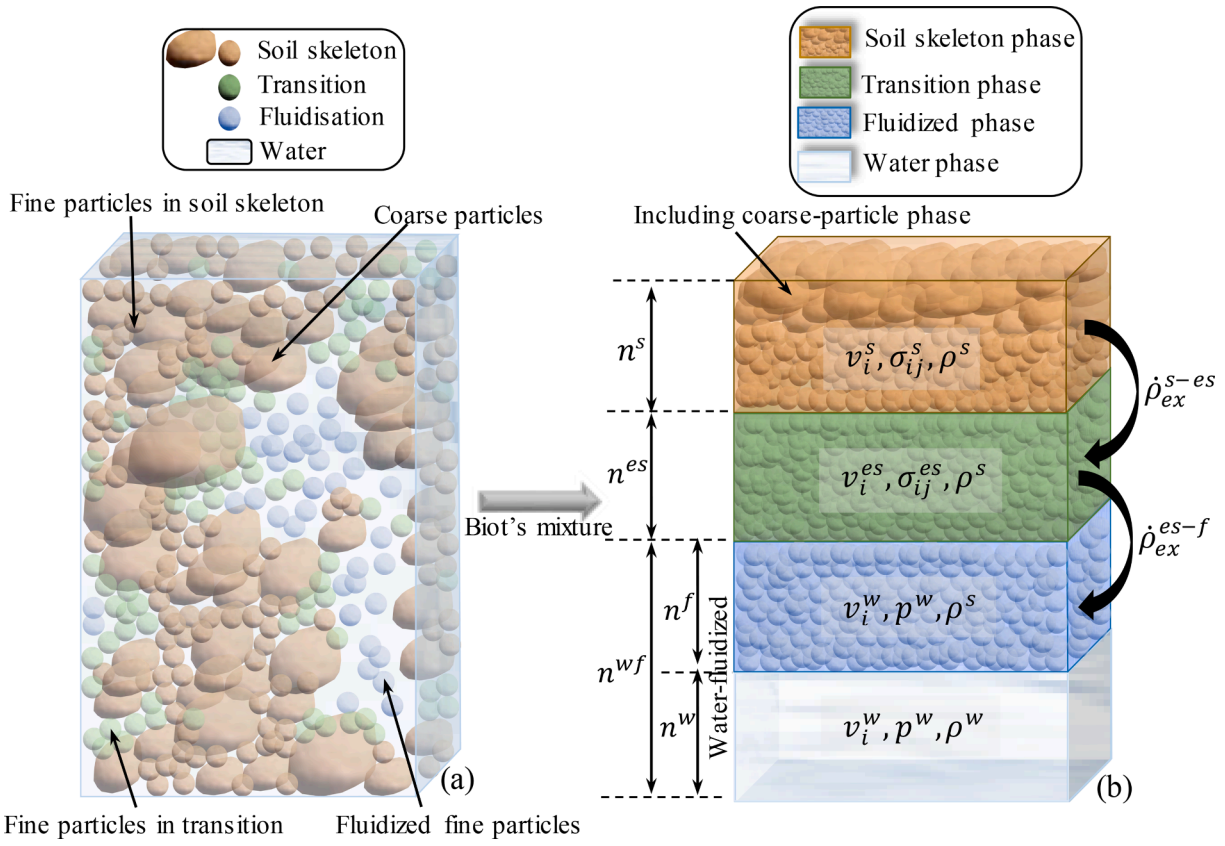

Fig. 3. Continuum approximation of fully saturated porous media (a) Eroded soil configuration (b) Phase assumption.

3.1. Mass conservation equations

This section presents the derivation of mass conservation laws for individual phases of the mixture based on the Reynolds transport theorem. A part of the solid phase is transformed into the transition phase and then mobilized grains in the seepage flow during internal erosion. Thus, there are terms representing mass exchanges $\dot{\rho}_{ex}^{\vartheta}$ between three phases (ϑ denoting "$s-es$" or "$es-f$"). Given this observation, the generic form of mass conservation law for the $\varkappa$-phase can be expressed through the Reynolds transport theorem as follows:

$$\frac{d^{\varkappa}}{dt}\int_V \overline{\rho}^{\varkappa} dV = \int_V \dot{\rho}_{ex}^{\vartheta} dV \tag{6}$$

Or,

$$\int_V \left[\frac{\partial \overline{\rho}^{\varkappa}}{\partial t} + v_i^{\varkappa}\frac{\partial \overline{\rho}^{\varkappa}}{\partial x_i} + \overline{\rho}^{\varkappa}\frac{\partial v_i^{\varkappa}}{\partial x_i}\right] dV = \int_V \dot{\rho}_{ex}^{\vartheta} dV \tag{7}$$

Thanks to the arbitrary property of V, we can rewrite Eq. (7) as:

$$\frac{D^{\varkappa}\overline{\rho}^{\varkappa}}{Dt} = -\overline{\rho}^{\varkappa}\frac{\partial v_i^{\varkappa}}{\partial x_i} + \dot{\rho}_{ex}^{\vartheta} \tag{8}$$

From Eq. (8) and by using the assumption of the sufficiently small changes of volume fractions with the location within the soil body (e.g. $\frac{\partial n^{\varkappa}}{\partial x_i} \approx 0$) (Oka et al., 2010; Einav and Liu, 2018; Bui and Nguyen, 2017), the mass conservation of three constituents with respect to the motion of solid skeleton takes the following forms:

$$\frac{D^s\overline{\rho}^s}{Dt} = -\overline{\rho}^s\frac{\partial v_i^s}{\partial x_i} - \dot{\rho}_{ex}^{s-es} \tag{9}$$

$$\frac{D^{es}\overline{\rho}^{es}}{Dt} = \frac{D^s\overline{\rho}^{es}}{Dt} = -\overline{\rho}^{es}\frac{\partial v_i^{es}}{\partial x_i} + \dot{\rho}_{ex}^{s-es} - \dot{\rho}_{ex}^{es-f} \tag{10}$$

$$\frac{D^{wf}\overline{\rho}^{wf}}{Dt} = \frac{D^s\overline{\rho}^{wf}}{Dt} = -\overline{\rho}^{wf}\frac{\partial v_i^w}{\partial x_i} + \dot{\rho}_{ex}^{es-f} \tag{11}$$

Taking $\rho^s = const$ and $\rho^w = const$, while using $\overline{\rho}^{\varkappa} = n^{\varkappa}\rho^{\varkappa}$, Eqs. (9) to (11) can be rewritten as:

$$\dot{n}^s = -n^s\frac{\partial v_i^s}{\partial x_i} - \frac{\dot{\rho}_{ex}^{s-es}}{\rho^s} \tag{12}$$

$$\dot{n}^{es} = -n^{es}\frac{\partial v_i^{es}}{\partial x_i} + \frac{\dot{\rho}_{ex}^{s-es}}{\rho^s} - \frac{\dot{\rho}_{ex}^{es-f}}{\rho^s} \tag{13}$$

$$\rho^s\dot{n}^f + \rho^w\dot{n}^w = -\left(\rho^s n^f + \rho^w n^w\right)\frac{\partial v_i^w}{\partial x_i} + \dot{\rho}_{ex}^{es-f} \tag{14}$$

In the above expressions, we use the superposed dot in $\dot{n}^{\varkappa}$ for simplicity to replace $\frac{D^s n^{\varkappa}}{Dt}$ representing the rate of volume fractions of each phase with respect to the motion of the solid skeleton.

The mass of the original water phase within the water-fluidized phase is always conservative in porous media as shown in the following form:

$$\frac{D^w\overline{\rho}^w}{Dt} = \frac{D^s\overline{\rho}^w}{Dt} = -\overline{\rho}^w\frac{\partial v_i^w}{\partial x_i} \tag{15}$$

It is illustrated in Eq. (15) that there is no mass exchange between the original water phase and others. Manipulating Eq. (15) in the form of the superposed dot in $\dot{n}^{\varkappa}$ with the assumption of $\rho^w = const$ and substituting it into Eq. (14), one obtains:

$$\dot{n}^w = -n^w\frac{\partial v_i^w}{\partial x_i} \tag{16}$$

$$\dot{n}^f = -n^f\frac{\partial v_i^w}{\partial x_i} + \frac{\dot{\rho}_{ex}^{es-f}}{\rho^s} \tag{17}$$

These two above expressions can be combined to obtain the following expression:

$$\dot{n}^{wf} = -n^{wf}\frac{\partial v_i^w}{\partial x_i} + \frac{\dot{\rho}_{ex}^{es-f}}{\rho^s} \tag{18}$$

It can be assumed that the inflow and outflow of erodible fine particles in the transition phase have the same mass ($\dot{\rho}_{ex}^{s-es} = \dot{\rho}_{ex}^{es-f} = \dot{\rho}_{ex}$) so that their exchange terms are assumed to sum to zero, allowing Eqs. (12) to (13) and Eq. (18) to be rewritten as:

$$\dot{n}^{s} = -n^{s}\frac{\partial v_i^s}{\partial x_i} - \frac{\dot{\rho}_{ex}}{\rho^s} \tag{19}$$

$$\dot{n}^{es} = -n^{es}\frac{\partial v_i^{es}}{\partial x_i} \tag{20}$$

$$\dot{n}^{wf} = -n^{wf}\frac{\partial v_i^w}{\partial x_i} + \frac{\dot{\rho}_{ex}}{\rho^s} \tag{21}$$

Given $n^s + n^{es} + n^{wf} = 1$, adding Eqs. (19) to (21) results in:

$$n^{wf}\delta_{ij}\frac{\partial v_i^w}{\partial x_j} = -n^s\delta_{ij}\frac{\partial v_i^s}{\partial x_j} - n^{es}\delta_{ij}\frac{\partial v_i^{es}}{\partial x_j} \tag{22}$$

Eqs. (19) to (22) represent the reciprocity between incremental forms of volume fraction and volumetric strain thanks to the assumption of incompressible soil skeleton.

3.2. Momentum equations

The momentum of a constituent is conservative in the sense that the momentum change is equal to the total external force on its volume (Chen et al., 2021). This is reflected through the following form:

$$\frac{d^\varkappa}{dt}\int_V \overline{\rho}^\varkappa v_i^\varkappa dV = -\int_S \left(\overline{\sigma}_{ij}^\varkappa n_j\right) dS + \int_V \overline{\rho}^\varkappa B_i dV + \int_V R_i^\varkappa dV \tag{23}$$

In the above equation, $\overline{\sigma}_{ij}^\varkappa n_j$ represents the partial traction force acting on the surface area dS of volume V with n_j being the outward unit normal vector on this surface (e.g. negative sign indicating the compressive positive conventions of the stresses), B_i is the body force of the mass $\overline{\rho}^\varkappa dV$ induced by the gravity acceleration constant g and $R_i^\varkappa$ denotes the viscous drag force acting on the $\varkappa$-phase.

We adopt the Reynolds transport theorem and the material time derivative of $\overline{\rho}^\varkappa$ and $v_i^\varkappa$ for the left-hand side term of Eq. (23) to obtain:

$$\frac{d^\varkappa}{dt}\int_V \overline{\rho}^\varkappa v_i^\varkappa dV = \int_V \left[v_i^\varkappa\left(\frac{D^\varkappa\overline{\rho}^\varkappa}{Dt} + \overline{\rho}^\varkappa\frac{\partial v_i^\varkappa}{\partial x_i}\right) + \overline{\rho}^\varkappa\frac{D^\varkappa v_i^\varkappa}{Dt}\right] dV \tag{24}$$

From Eqs. (8) and (24), the following relation can be obtained:

$$\frac{d^\varkappa}{dt}\int_V \overline{\rho}^\varkappa v_i^\varkappa dV = \int_V \left(v_i^\varkappa\dot{\rho}_{ex}^\vartheta + \overline{\rho}^\varkappa\frac{D^\varkappa v_i^\varkappa}{Dt}\right) dV \tag{25}$$

Using the Gauss theorem and comparing Eqs. (25) and (23) result in the balance of linear momentum for phase $\varkappa$ as follows:

$$\int_V \left(v_i^\varkappa\dot{\rho}_{ex}^\vartheta + \overline{\rho}^\varkappa\frac{D^\varkappa v_i^\varkappa}{Dt}\right) dV = -\int_V \frac{\partial\overline{\sigma}_{ij}^\varkappa}{\partial x_j} dV + \int_V \overline{\rho}^\varkappa B_i dV + \int_V R_i^\varkappa dV \tag{26}$$

which can become the following expression due to the arbitrary property of V:

$$\overline{\rho}^\varkappa\frac{D^\varkappa v_i^\varkappa}{Dt} = -\frac{\partial\overline{\sigma}_{ij}^\varkappa}{\partial x_j} + \overline{\rho}^\varkappa B_i + R_i^\varkappa - v_i^\varkappa\dot{\rho}_{ex}^\vartheta \tag{27}$$

The seepage flow is assumed to be laminar in the case of low water velocities, while the velocity of the solid is usually small within the porous media. Therefore, the acceleration of all phases and macroscopic viscous effects are considered to be sufficiently inconsiderable (e.g. $\frac{D^\varkappa v_i^\varkappa}{Dt} \approx 0$) (Borja and White, 2010; Gray et al., 2010). By applying this assumption and using $\dot{\rho}_{ex}^\vartheta = \dot{\rho}_{ex}$ as mentioned in Eqs. (19) to (21), the momentum balance of each phase in Eq. (27) can be written as:

$$-\frac{\partial\overline{\sigma}_{ij}^s}{\partial x_j} + \overline{\rho}^s B_i = -R_i^s - v_i^s\dot{\rho}_{ex} \tag{28}$$

$$-\frac{\partial\overline{\sigma}_{ij}^{es}}{\partial x_j} + \overline{\rho}^{es} B_i = -R_i^{es} \tag{29}$$

$$-\frac{\partial\overline{\sigma}_{ij}^{wf}}{\partial x_j} + \overline{\rho}^{wf} B_i = -R_i^{wf} + v_i^w\dot{\rho}_{ex} \tag{30}$$

The above expressions and Eqs. (19) to (22) are considered basic governing equations of the separate phases. They are then used to construct the formulation of work input with influences of the internal erosion process, reproducing the gain or loss of mass and the interaction of constituents within a heterogeneous system.

3.3. Work input

The work input is needed to consider the intrinsic transition of the state of fine particles at the grain scale, bridging their states from being attached to soil skeleton to fluidized. It can be reflected in the simultaneous activation and evolution of three phases within a short period observed at the continuum level, as illustrated in Figs. 1 and 2. This nature requires the interdependence of mechanical, seepage and erosion responses, leading to a unified work input of mixture representing the coupled hydro-mechanical responses, as described in the following formulations.

Utilizing homogenization reasoning, the power input L to any arbitrary volume fixed in space is obtained from the sum of the products of the various forces acting on the material with their respective velocities (Houlsby, 1979; Houlsby, 1997), taking the form below:

$$\int_V L dV = -\int_S \left(\overline{\sigma}_{ij}^s v_i^s + \overline{\sigma}_{ij}^{es} v_i^{es} + \overline{\sigma}_{ij}^{wf} v_i^w\right) n_j dS + \int_V \left(\overline{\rho}^s B_i v_i^s + \overline{\rho}^{es} B_i v_i^{es} + \overline{\rho}^{wf} B_i v_i^w\right) dV \tag{31}$$

in which the negative sign (e.g. $-\int_s \left(\overline{\sigma}_{ij}^s v_i^s + \overline{\sigma}_{ij}^{es} v_i^{es} + \overline{\sigma}_{ij}^{wf} v_i^w\right) n_j dS$) is used to represent the compressive positive conventions of the stresses.

Using the divergence theorem of Gauss and the arbitrary property of V in Eq. (31) leads to the following expression:

$$L = -\overline{\sigma}_{ij}^s\frac{\partial v_i^s}{\partial x_j} - \overline{\sigma}_{ij}^{es}\frac{\partial v_i^{es}}{\partial x_j} - \overline{\sigma}_{ij}^{wf}\frac{\partial v_i^w}{\partial x_j} + \left(-\frac{\partial\overline{\sigma}_{ij}^s}{\partial x_j} + \overline{\rho}^s B_i\right) v_i^s + \left(-\frac{\partial\overline{\sigma}_{ij}^{es}}{\partial x_j} + \overline{\rho}^{es} B_i\right) v_i^{es} + \left(-\frac{\partial\overline{\sigma}_{ij}^{wf}}{\partial x_j} + \overline{\rho}^{wf} B_i\right) v_i^w \tag{32}$$

Combining Eqs. (28) to (30) and (32) results in:

$$L = -\overline{\sigma}_{ij}^s\frac{\partial v_i^s}{\partial x_j} - \overline{\sigma}_{ij}^{es}\frac{\partial v_i^{es}}{\partial x_j} - \overline{\sigma}_{ij}^{wf}\frac{\partial v_i^w}{\partial x_j} + \left(v_i^w v_i^w - v_i^s v_i^s\right)\dot{\rho}_{ex} - R_i^s v_i^s - R_i^{es} v_i^{es} - R_i^{wf} v_i^w \tag{33}$$

Due to $R_i^s + R_i^{es} + R_i^{wf} = 0$, Eq. (33) can be rewritten as:

$$L = -\overline{\sigma}_{ij}^s\frac{\partial v_i^s}{\partial x_j} - \overline{\sigma}_{ij}^{es}\frac{\partial v_i^{es}}{\partial x_j} - \overline{\sigma}_{ij}^{wf}\frac{\partial v_i^w}{\partial x_j} + \left(v_i^w v_i^w - v_i^s v_i^s\right)\dot{\rho}_{ex} + R_i^{es}\left(v_i^s - v_i^{es}\right) + R_i^{wf}\left(v_i^s - v_i^w\right) \tag{34}$$

By using Eq. (5), we can rewrite Eq. (34) as follows:

$$L = -\left(\sigma_{ij} - n^{es}\sigma_{ij}^{es} - n^{wf}p^w\delta_{ij}\right)\frac{\partial v_i^s}{\partial x_j} - n^{es}\sigma_{ij}^{es}\frac{\partial v_i^{es}}{\partial x_j} - n^{wf}p^w\delta_{ij}\frac{\partial v_i^w}{\partial x_j} + \left(v_i^w v_i^w - v_i^s v_i^s\right)\dot{\rho}_{ex} + R_i^{es}\left(v_i^s - v_i^{es}\right) + R_i^{wf}\left(v_i^s - v_i^w\right) \tag{35}$$

Substitution of Eq. (22) into Eq. (35) leads to:

$$L = -\left[\sigma_{ij} - p^w\delta_{ij} + n^{es}\left(p^w\delta_{ij} - \sigma_{ij}^{es}\right)\right]\frac{\partial v_i^s}{\partial x_j} + n^{es}\left(p^w\delta_{ij} - \sigma_{ij}^{es}\right)\frac{\partial v_i^{es}}{\partial x_j} + \left(v_i^w v_i^w - v_i^s v_i^s\right)\dot{\rho}_{ex} + R_i^{es}\left(v_i^s - v_i^{es}\right) + R_i^{wf}\left(v_i^s - v_i^w\right) \tag{36}$$

In the above expression, $-\frac{\partial v_i^s}{\partial x_j} = \dot{\varepsilon}_{ij}$ is the rate of the strain tensor where the negative sign results from the assumption of the compressive positive conventions of the strain. It can be assumed that the shear component of σ_{ij}^{es} are negligible due to weak contact forces between detachable particles and others immediately before detachment (Shire and O'Sullivan, 2013). In addition, the drag force R_i^{es} during the phase transition from solid to fluidized is small since this phase is considered an idealised immediate phase taking place within a very short time.

Given the above assumptions, Eq. (36) can be rewritten as:

$$L = \left[\sigma_{ij} - p^w\delta_{ij} + n^{es}(p^w - p^{es})\delta_{ij}\right]\dot{\varepsilon}_{ij} + n^{es}(p^w - p^{es})\delta_{ij}\frac{\partial v_i^{es}}{\partial x_j} + \left(v_i^w v_i^w - v_i^s v_i^s\right)\dot{\rho}_{ex} + R_i^{wf}\left(v_i^s - v_i^w\right) \tag{37}$$

where p^{es} is mean intrinsic stress of the transition phase.

What makes the current approach distinct from other existing works (Steeb and Diebels, 2003; Rousseau et al., 2020; Zhang et al., 2013) is the first and second terms of the right-hand side of Eq. (37) where $n^{es}(p^w - p^{es})\delta_{ij}$ appears. This term describes the change in effective stress associated with the loss of contacts during the transition of eroded solid from soil skeleton to fluidization. Further discussions on this feature will be followed in Section 4.

In Eq. (37), p^{es} and v_i^{es} are essential variables of the transition phase representing the phase transition of erodible particles. Nevertheless, it is difficult to include the time-dependent transition of p^{es} and v_i^{es} in tackling responses of erodible particles during the process of internal erosion in terms of continuum models due to the lack of experimental data at the micro scale. It is noted that this transition process usually takes place suddenly, as illustrated in grain scale simulations (Liu et al., 2020, Zhou et al., 2020). Thus, assumptions on forms of p^{es} and v_i^{es} are essential for the development of a theoretical framework. It is acknowledged that these assumptions should strike a balance between rigour, performance and simplicity to describe necessary behavioural features of soils to make them more accessible to practical engineering. Given the transition between solid and fluid-like states, it is reasonable to assume p^{es} and v_i^{es} as follows:

$$p^{es} = \alpha p^w + (1-\alpha)p^s \tag{38}$$

$$v_i^{es} = \beta v_i^w + (1-\beta)v_i^s \tag{39}$$

where p^s is the mean intrinsic stress of solid phase.

Using parameters α and β in Eqs. (38) and (39) is considered as a simple way to demonstrate how the transition process can be incorporated into the constitutive formulation over a continuum time scale. They control the transition in stress and velocity between solid and fluid-like phases of erodible particles during erosion processes. In other words, parameters α and β are the consequences of the introduction of the transition phase in continuum modelling. Their values (ranging from 0 to 1) allow describing how fast or slow the internal erosion process is. For example, the combinations of different values of α and β enables us to flexibly describe different extreme cases of internal erosion (i) entirely-eroded transition phase (fluid-like) (ii) no erosion at all (the transition phase holds pressure and velocity of solid skeleton) (iii) a very fast transition (a sudden loss of fine grains holding very high stresses which are "instantly" washed out by fluid) (iv) a very slow erosion process (transition phase holding fluid pressure, but still moving with the solid skeleton). Further details can be found in Section 4.2. This treatment is believed to be acceptable as long as these two parameters can be identified and calibrated using standard tests, and the calibrated models can reproduce the experimental trends over a range of mechanical and hydraulic conditions under effects of erosion. This is one of our planned investigations in future papers on internal erosion.

Substituting Eqs. (38) and (39) into Eq. (37) allows us to rewrite Eq. (37) as follows:

$$L = \left\{\sigma_{ij} - p^w\delta_{ij} + \frac{(1-\alpha)\beta n^{es}}{(\beta n^{es} + n^{wf})}(p^w - p^s)\delta_{ij}\right\}\dot{\varepsilon}_{ij} + \left(v_i^w v_i^w - v_i^s v_i^s\right)\dot{\rho}_{ex} + R_i^{wf}\left(v_i^s - v_i^w\right) \tag{40}$$

For further expansion of Eq. (40), Eq. (5) can be recalled in the form of the total mean stress p as follows:

$$p = n^s p^s + n^{es} p^{es} + n^{wf} p^w \tag{41}$$

From Eqs. (41) and (38), the intrinsic pressure of the solid phase can take the following form:

$$p^s = \frac{p - (\alpha n^{es} + n^{wf})p^w}{n^s + (1-\alpha)n^{es}} \tag{42}$$

which can be substituted into Eq. (40) to obtain the form below:

$$L = \left\{\sigma_{ij} - p^w\delta_{ij} + \frac{(1-\alpha)\beta n^{es}}{(\beta n^{es} + n^{wf})[n^s + (1-\alpha)n^{es}]}(p^w - p)\delta_{ij}\right\}\dot{\varepsilon}_{ij} + \left(v_i^w v_i^w - v_i^s v_i^s\right)\dot{\rho}_{ex} + R_i^{wf}\left(v_i^s - v_i^w\right) \tag{43}$$

On the other hand, the body force of the mass can be neglected ($B_i \approx 0$) in Eq. (30). The viscous drag force of R_i^{wf} acting on the *wf*-phase can be assumed to be equal to R_i^f of the fluidized phase, due to the mix of eroded particles and water within the seepage flow:

$$R_i^{wf} = R_i^w = n^w\frac{\partial p^w}{\partial x_i} \tag{44}$$

Substituting the above expression into Eq. (43), we obtain:

$$L = \sigma_{ij}'\dot{\varepsilon}_{ij} + p_e'\dot{\rho}_{ex} + \frac{\partial p^w}{\partial x_i}\theta_i = \left\{\sigma_{ij} - p^w\delta_{ij} + \frac{(1-\alpha)\beta n^{es}}{(\beta n^{es} + n^{wf})[n^s + (1-\alpha)n^{es}]}(p^w - p)\delta_{ij}\right\}\dot{\varepsilon}_{ij} + \left(v_i^w v_i^w - v_i^s v_i^s\right)\dot{\rho}_{ex} + \frac{\partial p^w}{\partial x_i}n^w\left(v_i^s - v_i^w\right) \tag{45}$$

where $\sigma_{ij}' = \sigma_{ij} - p^w\delta_{ij} + \frac{(1-\alpha)\beta n^{es}}{(\beta n^{es} + n^{wf})[n^s + (1-\alpha)n^{es}]}(p^w - p)\delta_{ij}$, $p_e' = v_i^w v_i^w - v_i^s v_i^s$ and $\theta_i = n^w\left(v_i^s - v_i^w\right)$ are effective stress, erosion-driving force and water flux, respectively.

The formulations in Section 3 present a derivation of work input accounting for the most fundamental features of the coupling between the matrix of porous material and fluid flow in the case of internal erosion. Our formulation aims to obtain a good balance between rigour and simplicity. It is expected to form a basis for the development of constitutive models taking into account internal erosion (see Section 4.3). The above expressions allow quantifying the amounts of hydraulic and mechanical energy produced or dissipated within the total budget of work input by conjugate pairs. This is associated with the simultaneous processes of deformation, erosion and seepage, hence reflecting essential hydro-mechanical responses under the effects of erosion. Our proposed work input includes the effects of the transformation process between soil skeleton and fluidized states, as key difference with other existing forms of work input for soils undergoing internal erosion. It can be seen that the proposed form of the work input can automatically become the classical form for fully saturated soils (Houlsby, 1979) if $\dot{\rho}_{ex} = 0$ and $n^{es} = 0$, capturing the transition between states of non-eroded and eroded soils.

4. How to use the proposed work input in constitutive modelling of soils undergoing erosion

In this section, some discussions are made to gain a general picture of

how the proposed work input can be used for developing continuum models to capture the hydromechanical coupling of saturated soils under the effects of internal erosion.

4.1. Work conjugate pairs

Our proposed formulation is expected to provide an appropriate choice of work conjugate variable pairs reflecting interaction and transition between solid and water phases during internal erosion. This is essential for the development of constitutive models for describing the coupling between mechanical response, fluid transport and erosion process (e.g. see Section 4.3) under various loading, hydraulic and erosion cases.

The proposed form of work input reflects underlying micromechanisms of deformation, fluid transport and erosion. The underlying micromechanical quantities and their interactions are represented at the macro scale by macroscopic stress-like variables (e.g. σ'_{ij}, $\frac{\partial p^w}{\partial x_i}$ and p'_e) in continuum modelling. Effective stress σ'_{ij} is the stress on soil skeleton governed by contact forces between particles. The seepage force $\frac{\partial p^w}{\partial x_i}$ is to describe coupled solid deformation-fluid flow in fully saturated porous media. $\frac{\partial p^w}{\partial x_i}$ is one of the main components in governing the overall rate of energy loss associated with friction at the water-solid interphase (Houlsby, 1979; Houlsby, 1997). The erosion-driving force p'_e is related to the kinematic energy controlling the process of mass loss due to detachment of fine grains. Given its appearance in the expression of work input, p'_e should appear in criteria for activation and evolution of internal erosion.

The above effective stress σ'_{ij}, fluid pressure gradient $\frac{\partial p^w}{\partial x_i}$ and erosion-driving p'_e, are work conjugated with strain $\dot{\varepsilon}_{ij}$ (Borja and Koliji, 2009; Song and Silling, 2020), water flux θ_i and mass loss $\dot{\rho}_{ex}$, respectively, associated with a change in the system state. Apart from strain rate $\dot{\varepsilon}_{ij}$ and water flux θ_i in the traditional form of work input (Houlsby, 1979; Houlsby, 1997), the mass loss $\dot{\rho}_{ex}$ appears as an additional variable associated with erosion representing the rate of mass loss induced by seepage flow.

4.2. Effective stress accounting for the process of internal erosion

Effective stress can be considered as the stress at the inter-particle contacts, related to the deformation and failure of the soil skeleton, and governed by both the external load and contact-level action (Loret and Khalili, 2002; Andrade et al., 2022; Duriez et al., 2017). According to Houlsby (1997), Borja and Koliji (2009) and Coussy et al (2010), the effective stress is work conjugated with the strain rate of the solid skeleton, indicating mechanical work input associated with changes in the soil skeleton. Accordingly, the traditional form of Terzaghi's effective stress (Andrade et al., 2022; Duriez et al., 2017; Jiang et al., 2017; Selvadurai and Suvorov, 2016; Serpieri et al., 2015) or its extended form accounting for the Biot coefficient (Borja and Koliji, 2009; Benallal and Claudia, 2003; El Tabbal et al., 2020; Gawin et al., 2020; Aichi and Tokunaga, 2012) have been widely used for porous media. However, loss of contacts of fine particles due to erosion induces changes to the soil skeleton and these changes should be reflected in the effective stress. In this sense, it can be argued that the form of Terzaghi's effective stress usually used for internal erosion (e.g. Steeb and Diebels, 2003; Rousseau et al., 2020; Zhang et al., 2013) may not faithfully represent the effect of internal erosion on soil skeleton. Missing details on the transition phase is the key here. This is because the lateral support of fine particles in the force chain of the soil skeleton is suddenly lost during the state transition process of fine particles from solid to fluidization. Such a transition results in the development of the buckling of the chained particles and then the variation in the averaged effective stress. This behavioural feature can be addressed by our new form of effective stress drawn from Eq. (45) as follows:

$$\sigma'_{ij} = \overbrace{\sigma_{ij} - p^w\delta_{ij}}^{Terzaghi's\ effective\ stress} + \overbrace{\frac{(1-\alpha)\beta n^{es}}{(\beta n^{es} + n^{wf})[n^s + (1-\alpha)n^{es}]}(p^w - p)\delta_{ij}}^{Erosion-induced\ term} \tag{46}$$

Eq. (46) indicates that our current effective stress tensor consists of two components: Terzaghi's effective stress and Erosion-induced term. The second component accounts for the transition of erodible particles before and after fluidization (see Part II in Eq. (46)). The volume fraction n^{es} of the transition phase represents the amount of fine grains ready to detach from the soil skeleton induced by the seepage flow. These fine grains are in weak force chains which, in Discrete Element Methods, can be identified when their contact forces are smaller than the average contact force (e.g. Radjai et al., 1998; Nie et al., 2020) or with inconsiderable deviatoric stresses (e.g. Thornton and Antony, 1998; Shire and O'Sullivan, 2013). Weakly connected grains have a minor contribution to the force transmission in the soil skeleton and are progressively disrupted upon seepage forces of water flow, going with releasing the strain energy stored in contacts (Liu et al., 2020). In principle, micromechanical approaches allow detecting whether particles are in all low-connectivity particles in the heterogeneous network of particle contacts (Shire et al., 2014; Ma et al., 2021). From this, the number of weakly connected particles and corresponding volume fraction can be then computed.

The effect of n^{es} on the normalised mean effective stress $\frac{p'}{p-p^w} = 1 - \frac{(1-\alpha)\beta n^{es}}{[1-n^s-(1-\beta)n^{es}][n^s+(1-\alpha)n^{es}]}$ can be seen in Fig. 4, using $\alpha = 0.5$ and $\beta = 0.5$. As can be seen in Fig. 4, the nominalised mean effective stress decreases with increasing n^{es}. This indicates considerable effect of the transition phase on the stress of the soil skeleton, reflecting the dependence of soil strength on the size of weak contact networks. The range of n^{es} requires DEM-CFD analyses and will be considered in future works.

Parameters α and β in the expression of effective stress are used to control the transition process and hence the effects of erosion on effective stress. Recalling Eq. (38), $0 < \alpha < 1$ indicates that for the considered state, the averaged pressure p^{es} of the transition phase is lower than the mean intrinsic pressure p^s of the solid skeleton (assuming fluid pressure is smaller than p^s). Therefore a fraction of this phase can potentially be washed away if the hydraulic gradient is high enough. It is noted that the volume fraction of the transition phase indicates the total amount of fine grains that can be potentially eroded at a given instant. It does not mean the whole phase will be eroded at once. In a similar sense, $0 < \beta < 1$ in Eq. (39) reflects how fast or slow the erosion process is, with the transition phase transforming from solid to fluidized state. The combination of α and β allows describing the effects of erosion on effective stress and extreme cases (see Fig. 5). It is noted that the particles in Fig. 5 are indicative for illustration purposes only, given we are working on quantities at continuum scale, following Biot's mixture theory. The extreme cases in Fig. 5 are described below:

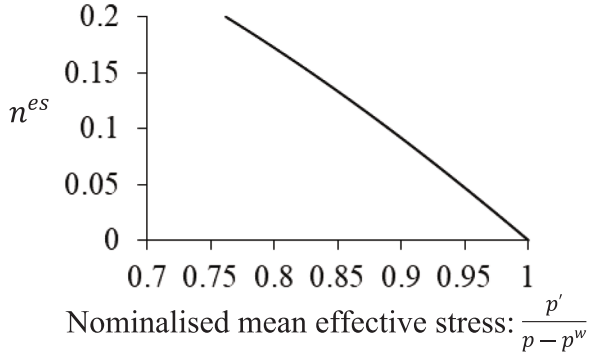

Fig. 4. Variation in nominalised mean effective stress against n^{es} at $\alpha = 0.5$ and $\beta = 0.5$

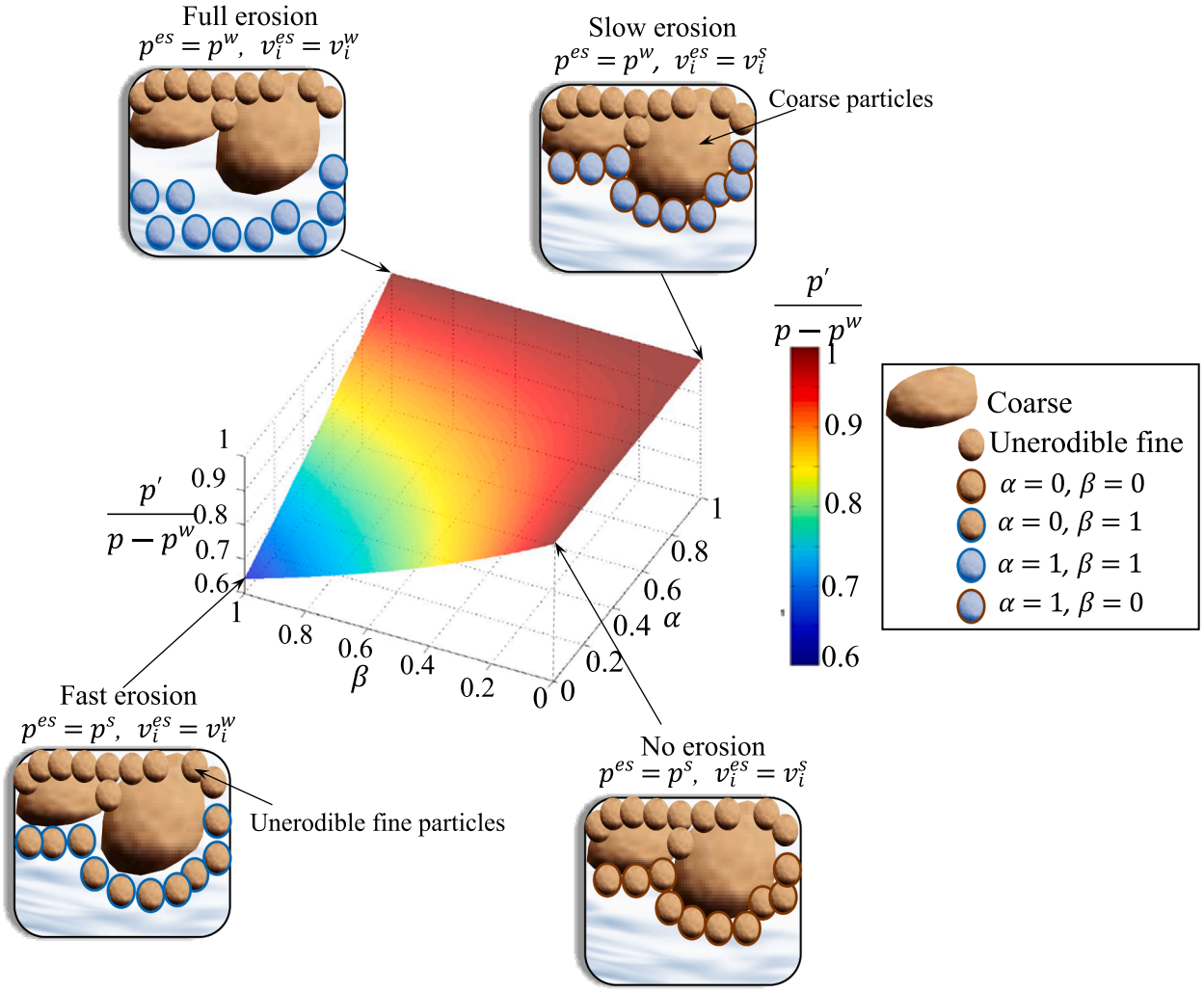

Fig. 5. Extreme cases of erosion and how fast or slow the transition from solid to fluidized is (through different values of α and β; see Eqs. (38) and (39)) at $n^{es} = 0.1$.

a) The effective stress can reduce to the classical Terzaghi's form when $\alpha = 1$ and $\beta = 1$, indicating that the whole transition phase has been eroded, given its intrinsic pressure and velocity coincide with the fluid's counterparts. On the other hand, the same classical Terzaghi's effective stress is obtained for $\alpha = 0$ and $\beta = 0$, in which the transition phase holds pressure and velocity of solid skeleton, indicating no erosion at all. It is noted that the evolution of effective stress is linked with the evolution of shear strength due to erosion, and although in both extreme cases ($\alpha = 1, \beta = 1$, and $\alpha = 0, \beta = 0$) Terzaghi's effective stress is recovered, the former ($\alpha = 1, \beta = 1$) is associated with lower shear strength given the loss of fine particles due to erosion.

b) The influence of erosion on effective stress is most profound if there is a sudden loss of fine grains holding very high stresses, represented by $\alpha = 0$ (e.g. $p^{es} = p^s$), which are "instantly" washed out by fluid, represented by $\beta = 1$ (e.g. $v_i^{es} = v_i^w$). Such cases indicate a very fast transition: sudden loss of total energy hold by transition phase to fluid phase. Fig. 6 shows such effects for different values of n^{es}.

c) A very slow erosion process, represented by $\alpha = 1$ and $\beta = 0$ (transition phase holding fluid pressure, but still moving with the solid skeleton), leads to no influence on effective stress, as seen in Fig. 5.

Other combinations of α and β to represent the stress state and velocity of transition phase can be used to describe how fast or slow erosion process is. As can be seen, the formulation results in three key parameters, n^{es}, α and β, and their effect on effective stress of the soil skeleton. The prospect of using all these three key parameters, as variables to describe the evolution of erosion process and its effect on shear strength at continuum scale will need further investigations and cannot be covered in this study.

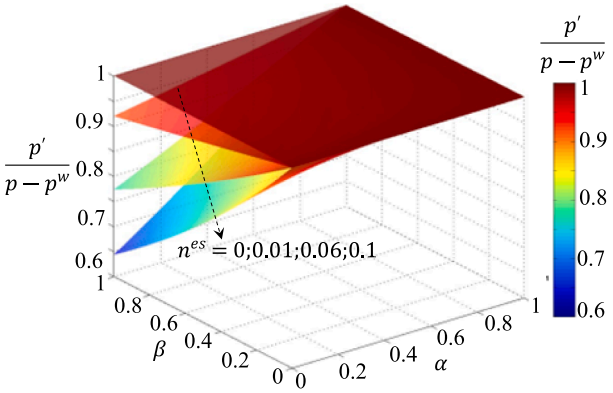

Fig. 6. Effect on mean effective stress, due to the amount of transition phase in the system, using $n^{es} = 0$, 0.01, 0.06 and 0.1.

The combined effect of all parameters, n^{es}, α and β, on effective stress are presented in Fig. 6. Stronger effect can be seen for increasing value of n^{es}, indicating soils that are more susceptible to erosion. In combination

with parameters α and β that characterise the pressure and velocity of the transition phase, the effect n^{es} can be accelerated or negated depending on how the erosion processs is, e.g. fast or slow.

4.3. Formulating constitutive models accounting for seepage, plasticity and erosion criteria

The behaviour of eroded soils is experimentally observed in the interdependence and transformation between fine and fluid phases due to mass loss. These mutual solid-fluid transformations and interactions are intrinsically governed by four main factors: soil susceptibility, stress condition, loading path, and hydraulic gradient. They all must be essentially taken into account in plasticity, seepage and erosion criteria for representing the hydro-mechanical behaviour in constitutive modelling as described in this section through an example of generic criteria.

4.3.1. Fundamental relationships

The derivation of plasticity, seepage and erosion criteria can start with the obtained rate of work input (see Eq. (45)) written in the triaxial form as follows:

$$\begin{aligned} L &= p^{'}\dot{\varepsilon}_{\nu} + q\dot{\varepsilon}_{s} + \rho^{u}_{ex}p^{'}_{e}\dot{E} + \frac{\partial p^{w}}{\partial x_i}\theta_i \\ &= \left\{ p - p^{w} + \frac{(1-\alpha)\beta n^{es}}{(\beta n^{es} + n^{wf})[n^{s} + (1-\alpha)n^{es}]}(p^{w} - p)\delta_{ij} \right\}\dot{\varepsilon}_{\nu} + q\dot{\varepsilon}_{s} + \\ &+ \rho^{u}_{ex}\left(v^{w}_{i}v^{w}_{i} - v^{s}_{i}v^{s}_{i}\right)\dot{E} + \frac{\partial p^{w}}{\partial x_i}n^{w}\left(v^{s}_{i} - v^{w}_{i}\right) \end{aligned} \tag{47}$$

where $E = \frac{\rho_{ex}}{\rho^{u}_{ex}}$ is the erosion index defined as the ratio between the current mass loss ρ_{ex} and ultimate mass loss ρ^{u}_{ex}; ε_{ν} is the volumetric strain; ε_s is the deviatoric strain; $p^{'}$ is the effective mean stress and q is the deviatoric stress. The triaxial stresses $(p^{'}, q)$ and triaxial strains $(\varepsilon_{\nu}, \varepsilon_s)$ can be expressed in the following forms of Cauchy effective stress $\left(\sigma^{'}_{ij}\right)$ and strain tensors $\left(\varepsilon_{ij}\right)$, respectively.

$$p^{'} = -\frac{1}{3}\sigma^{'}_{kk}, \text{and} q = \sqrt{\frac{3}{2}\left(\sigma^{'}_{ij} - \frac{1}{3}\sigma^{'}_{kk}\delta_{ij}\right)\left(\sigma^{'}_{ij} - \frac{1}{3}\sigma^{'}_{kk}\delta_{ij}\right)} \tag{48}$$

$$\varepsilon_{\nu} = -\varepsilon_{kk}, \text{and} \varepsilon_{s} = \sqrt{\frac{2}{3}\left(\varepsilon_{ij} - \frac{1}{3}\varepsilon_{\nu}\delta_{ij}\right)\left(\varepsilon_{ij} - \frac{1}{3}\varepsilon_{\nu}\delta_{ij}\right)} \tag{49}$$

The Helmholtz free energy can assume the general form below:

$$\psi = \mu(E)\psi^{m}\left(\varepsilon_{\nu}, \varepsilon_{s}, \varepsilon^{p}_{\nu}, \varepsilon^{p}_{s}\right) \tag{50}$$

In the above expression, ε^{p}_{ν} and ε^{p}_{s} are plastic volumetric and deviatoric strains, respectively. They are considered internal variables of plasticity. ψ^{m} is the Helmholtz free energy of uneroded soils. $\mu(E)$ is a function of E used for describing the effect of erosion on the elastic stiffness, where $\mu(E) = 1$ in the case of $E = 0$ (uneroded). In this sense E plays a similar role as a scalar damage indicator in Damage Mechanics (Lemaitre, 2012), or scalar breakage indicator in Breakage Mechanics theory (Einav, 2007a; Einav, 2007b; Das et al., 2014; Tengattini et al., 2014; Einav and Valdes, 2008; Nguyen and Einav, 2010). The specific forms of $\mu(E)$ requires micromechanical insights and are a subject of future investigation. For the presentation in this study, the generic form of $\mu(E)$ is used.

Therefore, the rate of Helmholtz free energy can be expressed as follows:

$$\dot{\psi} = \mu\left(\frac{\partial\psi^{m}}{\partial\varepsilon_{\nu}}\dot{\varepsilon}_{\nu} + \frac{\partial\psi^{m}}{\partial\varepsilon_{s}}\dot{\varepsilon}_{s} + \frac{\partial\psi^{m}}{\partial\varepsilon^{p}_{\nu}}\dot{\varepsilon}^{p}_{\nu} + \frac{\partial\psi^{m}}{\partial\varepsilon^{p}_{s}}\dot{\varepsilon}^{p}_{s}\right) + \frac{\partial\mu}{\partial E}\psi^{m}\dot{E} \tag{51}$$

Under isothermal conditions, the energy balance (Coussy, 2006), written for a volume element undergoing dissipative processes due to mechanical behaviour, seepage flow and internal erosion, is of the form:

$$L = \dot{\psi} + \widetilde{\Phi} = \mu\left(\frac{\partial\psi^{m}}{\partial\varepsilon_{\nu}}\dot{\varepsilon}_{\nu} + \frac{\partial\psi^{m}}{\partial\varepsilon_{s}}\dot{\varepsilon}_{s} + \frac{\partial\psi^{m}}{\partial\varepsilon^{p}_{\nu}}\dot{\varepsilon}^{p}_{\nu} + \frac{\partial\psi^{m}}{\partial\varepsilon^{p}_{s}}\dot{\varepsilon}^{p}_{s}\right) + \frac{\partial\mu}{\partial E}\psi^{m}\dot{E} + \widetilde{\Phi} \tag{52}$$

with $\widetilde{\Phi}$ being the dissipation potential.

By comparing Eqs. (52) and (47), the following fundamental relationships can be obtained:

$$p^{'} = \mu\frac{\partial\psi^{m}}{\partial\varepsilon_{\nu}} \tag{53}$$

$$q = \mu\frac{\partial\psi^{m}}{\partial\varepsilon_{s}} \tag{54}$$

and

$$\begin{aligned} \widetilde{\Phi} &= -\mu\frac{\partial\psi^{m}}{\partial\varepsilon^{p}_{\nu}}\dot{\varepsilon}^{p}_{\nu} - \mu\frac{\partial\psi^{m}}{\partial\varepsilon^{p}_{s}}\dot{\varepsilon}^{p}_{s} + \left(\rho^{u}_{ex}p^{'}_{e} + \frac{\partial\mu}{\partial E}\psi^{m}\right)\dot{E} - \frac{\partial p^{w}}{\partial x_i}\theta_i \\ &= \overline{\chi}^{\nu}\dot{\varepsilon}^{p}_{\nu} + \overline{\chi}^{s}\dot{\varepsilon}^{p}_{s} + \overline{\chi}^{e}\dot{E} + \overline{\chi}^{w}_{i}\theta_i \end{aligned} \tag{55}$$

in which the generalised stresses $\overline{\chi}^{\nu} = -\mu\frac{\partial\psi^{m}}{\partial\varepsilon^{p}_{\nu}}$, $\overline{\chi}^{s} = -\mu\frac{\partial\psi^{m}}{\partial\varepsilon^{p}_{s}}$, $\overline{\chi}^{e} = \rho^{u}_{ex}p^{'}_{e} + \frac{\partial\mu}{\partial E}\psi^{m}$ and $\overline{\chi}^{w}_{i} = -\frac{\partial p^{w}}{\partial x_i}$ are the thermodynamic conjugates to rates of volumetric plastic strain $\dot{\varepsilon}^{p}_{\nu}$, deviatoric plastic strain $\dot{\varepsilon}^{p}_{s}$, erosion index $\dot{E}$ and water flux θ_i, respectively.

The dissipation can also be written as follows:

$$\widetilde{\Phi} = \widetilde{\Phi}^{me} + \widetilde{\Phi}^{h} = \underbrace{\frac{\partial\widetilde{\Phi}}{\partial\dot{\varepsilon}^{p}_{\nu}}\dot{\varepsilon}^{p}_{\nu} + \frac{\partial\widetilde{\Phi}}{\partial\dot{\varepsilon}^{p}_{s}}\dot{\varepsilon}^{p}_{s} + \frac{\partial\widetilde{\Phi}}{\partial\dot{E}}\dot{E}}_{\dot{\Phi}^{me}} + \underbrace{\chi^{w}_{i}\theta_i}_{\dot{\Phi}^{h}} = \chi^{\nu}\dot{\varepsilon}^{p}_{\nu} + \chi^{s}\dot{\varepsilon}^{p}_{s} + \chi^{e}\dot{E} + \chi^{w}_{i}\theta_i \tag{56}$$

where χ^{ν}, χ^{s}, χ^{e} and χ^{w}_{i} are volumetric, deviatoric, erosion and hydraulic dissipative generalised stresses, respectively. It is noted that dissipations due to mechanical responses and erosion can be reasonably assumed rate-independent, resulting in first order homogeneous dissipation potential $\widetilde{\Phi}^{\text{me}}$ in terms of corresponding rates of internal variables (Houlsby and Puzrin, 2000; Houlsby and Puzrin, 2007). On the other hand, hydraulic dissipation is generally rate-dependent, and hence $\widetilde{\Phi}^{\text{h}}$ is not a homogeneous first order function in terms of the water flux $\theta_i = n^{w}\left(v^{s}_{i} - v^{w}_{i}\right)$. In that sense, a potential z^{w} is needed for the definition of χ^{w}_{i}, e.g. $\chi^{w}_{i} = \frac{\partial z^{w}}{\partial\theta_i}$. The details on rate-dependent dissipation processes due to hydraulic dissipation are not covered in this study. The readers can refer to Houlsby and Puzrin (2000), Houlsby and Puzrin (2007) for formulation of rate-dependent constitutive models based on thermodynamics.

Comparing Eq. (56) with Eq. (55), a form of Ziegler's orthogonality condition (Ziegler, 2012) can be obtained as:

$$\chi^{\nu} = \frac{\partial\widetilde{\Phi}}{\partial\dot{\varepsilon}^{p}_{\nu}} = \overline{\chi}^{\nu} = -\mu\frac{\partial\psi^{m}}{\partial\varepsilon^{p}_{\nu}} \tag{57}$$

$$\chi^{s} = \frac{\partial\widetilde{\Phi}}{\partial\dot{\varepsilon}^{p}_{s}} = \overline{\chi}^{s} = -\mu\frac{\partial\psi^{m}}{\partial\varepsilon^{p}_{s}} \tag{58}$$

$$\chi^{e} = \frac{\partial\widetilde{\Phi}}{\partial E} = \overline{\chi}^{e} = \rho^{u}_{ex}p^{'}_{e} + \frac{\partial\mu}{\partial E}\psi^{m} \tag{59}$$

$$\chi^{w}_{i} = \overline{\chi}^{w}_{i} = -\frac{\partial p^{w}}{\partial x_i} \tag{60}$$

4.3.2. A generic model

The evolutions of mechanical, hydraulic and erosion dissipative processes reflecting underlying grain-scale hydromechanical mechanisms can be incorporated into the model formulation through the approach by means of constraint equations. In this approach, dissipation potential takes the generic form set out below:

$$\widetilde{\Phi} = \varphi^{\nu}\dot{\varepsilon}_{\nu}^{\mathrm{p}} + \varphi^{s}\dot{\varepsilon}_{s}^{\mathrm{p}} + \varphi^{e}\dot{E} + \varphi_{i}^{w}\theta_{i} \geq 0 \tag{61}$$

In the above expression, φ^{ν}, φ^{s}, φ^{e} are generally functions of stresses, internal variables (plastic strain and E) and hydraulic gradient $\frac{\partial p^{w}}{\partial x_i}$, while and φ_i^{w} can be dependent on θ_i to reflect rate-dependent hydraulic dissipation. In this framework, to reflect kinematic interdependencies between two internal variables $\dot{\varepsilon}_{\nu}^{\mathrm{p}}$ and $\dot{\varepsilon}_{s}^{\mathrm{p}}$, the following kinematic constraint equation (C) is introduced:

$$C = B\dot{\varepsilon}_{\nu}^{\mathrm{p}} + A\dot{\varepsilon}_{s}^{\mathrm{p}} = 0 \tag{62}$$

where A and B are general functions associated with the dilation angle (Andrade et al., 2012; Borja, et al., 2013), governing dilation responses (Nguyen and Bui, 2020).

The kinematic constraint equation is also homogeneous first-order functions in terms of the rates of internal variables. Thanks to zero values, it can be used to supplement the dissipation potential to obtain an equivalent dissipation function using the standard method of Lagrangian multipliers (Houlsby and Puzrin, 2000) as follows:

$$\widetilde{\Phi} = \widetilde{\Phi} + \Lambda C = \varphi^{\nu}\dot{\varepsilon}_{\nu}^{\mathrm{p}} + \varphi^{s}\dot{\varepsilon}_{s}^{\mathrm{p}} + \varphi^{e}\dot{E} + \varphi_{i}^{w}\theta_{i} + \Lambda\left(B\dot{\varepsilon}_{\nu}^{\mathrm{p}} + A\dot{\varepsilon}_{s}^{\mathrm{p}}\right) \geq 0 \tag{63}$$

in which Λ is the Lagrangian kinematic multiplier. Using Eqs. (56) and (63), dissipative generalized stresses take the following forms:

$$\chi^{\nu} = \frac{\partial\widetilde{\Phi}}{\partial\dot{\varepsilon}_{\nu}^{\mathrm{p}}} = \varphi^{\nu} + B\Lambda \tag{64}$$

$$\chi^{s} = \frac{\partial\widetilde{\Phi}}{\partial\dot{\varepsilon}_{s}^{\mathrm{p}}} = \varphi^{s} + A\Lambda \tag{65}$$

$$\chi^{e} = \frac{\partial\widetilde{\Phi}}{\partial\dot{E}} = \varphi^{e} \tag{66}$$

$$\chi_{i}^{w} = \varphi_{i}^{w} \tag{67}$$

4.3.2.1. Seepage law. From Eqs. (67) and (60), the generic expression of seepage law can be obtained as follows:

$$\frac{\partial p^{w}}{\partial x_i} = -\varphi_{i}^{w} \tag{68}$$

which illustrates the hydraulic dissipation induced by the relative motion between solid and fluid phases and facilitates the establishment of Darcy's law if φ_i^{w} is assumed as a function of seepage velocity (e.g. θ_i) (Houlsby, 1979; Houlsby, 1997; Selvadurai and Suvorov, 2016). It is noted that this generic seepage law is only valid for the slow flow of a macroscopically inviscid fluid through fully saturated soils.

4.3.2.2. Plasticity criterion. By combining Eqs. (64) and (65), the loading function in the dissipative stress space $y^{*(m)}$ is obtained:

$$\chi_{\nu} = \varphi^{\nu} + \frac{B}{A}(\chi_{s} - \varphi^{s}) \tag{69}$$

A mechanical yield function $y^{*(m)}$ in generalised stress space (χ_{ν}, χ_{s}) can be obtained from Eq. (69) as:

$$y^{*(m)} = A\chi^{\nu} - B\chi^{s} - A\varphi^{\nu} + B\varphi^{s} \leq 0 \tag{70}$$

Along with this, the expressions for the mechanical flow rules are hence obtained as follows:

$$\dot{\varepsilon}_{\nu}^{\mathrm{p}} = \dot{\lambda}_{m}\frac{y^{*(m)}}{\partial\chi^{\nu}} = \dot{\lambda}_{m}A \tag{71}$$

$$\dot{\varepsilon}_{s}^{\mathrm{p}} = \dot{\lambda}_{m}\frac{y^{*(m)}}{\partial\chi^{s}} = -\dot{\lambda}_{m}B \tag{72}$$

where $\dot{\lambda}_m$ is the plasticity multiplier.

Eqs. (70) to (72) present a generic form of plasticity criterion in generalised stress space (χ_{ν}, χ_{s}) (see its illustration in Fig. 7) for saturated soils under the effects of internal erosion. χ_{ν} and χ_{s} are dependent on p', q and yield stress, allowing us to write Eqs. (70) to (72) in true stress space (p', q). A, B, φ^{ν} and φ^{s} can be assumed to be dependent on stresses (p', q), erosion (E) and hydraulic gradient ($\frac{\partial p^{w}}{\partial x_i}$) terms to capture the effects of hydraulic response and mass loss on the stress-strain behaviour. Thus, the yield surface for mechanical responses in true stress space can take the following generic form:

$$y^{(m)}\left(p', q, \frac{\partial p^{w}}{\partial x_i}, \varepsilon_{\nu}^{\mathrm{p}}, \varepsilon_{s}^{\mathrm{p}}, E\right) \leq 0 \tag{73}$$

It is noted that the derivation of the proposed plasticity criterion is based on the use of constraints in thermodynamic formulation. Alternatively, the special form of dissipation potential (Phan, 2021; Phan et al., 2021a; Phan et al., 2021b; Phan et al., 2023a; Phan et al., 2023b) can be adopted to construct a similar form of yield criterion.

4.3.2.3. Erosion criterion. To derive the erosion criterion based on our form of work input, Eq. (66) can be used to write the following erosion criterion in generalised dissipative stress space:

$$y^{*(e)} = \chi^{e} - \varphi^{e} \leq 0 \tag{74}$$

which leads to the following evolution rule for erosion:

$$\dot{E} = \dot{\lambda}_{e}\frac{y^{*(e)}}{\partial\chi^{e}} = \dot{\lambda}_{e} \tag{75}$$

with $\dot{\lambda}_e$ being the erosion multiplier.

Given $\chi^{e} = \rho_{ex}^{u}p_{e}' + \frac{\partial\mu}{\partial E}\psi^{m}$, the erosion criterion in true stress space is

$$y^{(e)} = \rho_{ex}^{u}p_{e}' + \frac{\partial\mu}{\partial E}\psi^{m} - \varphi^{e} \leq 0 \tag{76}$$

The erosion criterion can be furnished by the choices of φ^{e} where in general we can assume φ^{e} as a generic function of $p', q, \frac{\partial p^{w}}{\partial x_i}$ and E.

Eqs. (53), (54), (68), Eqs. (71) to (73) and Eqs. (75) to (76) represent the generic form of our model. In the proposed model, the assumption of transition phase may bring challenges for reaching a good validation between predictive and measured results on natural granular materials. The key challenge here is determination of variables (volume fraction, n^{es}) and calibration of parameters (α, β) related to the transition phase. At this stage, we acknowledge that there is a lack of adequate experimental data in existing laboratory that can provide sufficient details on these parameters and variables. The prospect of using them to describe

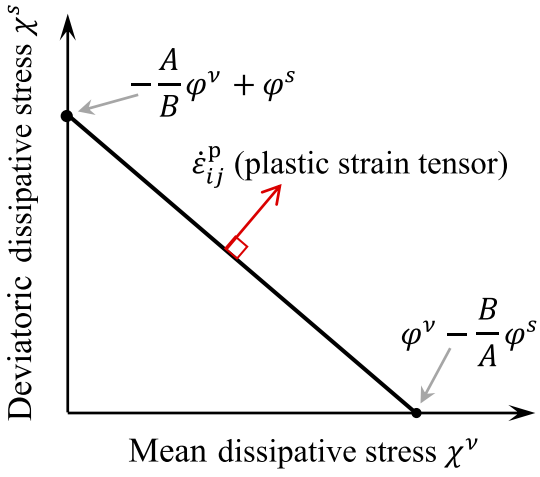

Fig. 7. Geometric representation of yield potential in dissipative stress for plasticity.

the evolution of erosion process and its effect at continuum scale will need further investigations.

The volume fraction of transition phase n^{es} can be computed based on gradients of solid and water velocities through Eq. (20) (mass conservation) but the assumption on the initial value of n^{es} is required and considered as a parameter. The appropriate ranges of the initial value of n^{es} is an important information for us to calibrate it. CFD-DEM simulations can be used for this calibration purpose where we can possibly identify number of fine grains in weak force chains and their corresponding volume fraction. Given the obtained range, the initial value of n^{es} can be adjusted together with values of α and β to allow model responses (e.g. stress-strain responses, and degree of erosion) to match with experimental data. It is, however, not yet adopted in this study, and left here as future work on the model development.

α and β reflect the transition speed (fast, slow, non-eroded, fully-eroded) through state properties of erodible particles closer to solid or fluid-like state. Thus, they can be adjusted within a range of 0 to 1 in the parameter calibration process so that macro quantities (stress, strain, degree of erosion) can match the experimental data at different levels of erosion.

4.3.3. Coupled hydro-mechanical-erosion tangent stiffness tensor

A consistent tangent stiffness matrix linking proposed stress-like variables and strain-like variables is one of the indispensable components in the development of a constitutive model. In the case of models for internal erosion, the tangent stiffness matrix can serve as an explicit indicator of the interaction between mechanical, hydraulic and mass loss processes in inelastic and erosion regimes, which can be shown in this section.

For the purpose of formulation derivation of the tangent stiffness, several essential formulations of the proposed generic model in Section 4.3.1 are first recalled. In particular, the generic stress-strain relationships can be assumed to be drawn from Eqs. (53) and (54) as follows:

$$p^{'} = \mu(E)\frac{\partial \psi^m}{\partial \varepsilon_v}\left(\varepsilon_v, \varepsilon_v^{\mathrm{p}}\right) \tag{77}$$

$$q = \mu(E)\frac{\partial \psi^m}{\partial \varepsilon_s}\left(\varepsilon_s, \varepsilon_s^{\mathrm{p}}\right) \tag{78}$$

From Eqs. (71) to (73), the yield function and evolution rules are of the following generic forms for plasticity:

$$y^{(m)}\left(p^{'}, q, \frac{\partial p^w}{\partial x_i}, \varepsilon_v^{\mathrm{p}}, \varepsilon_s^{\mathrm{p}}, E\right) \leq 0 \tag{79}$$

$$\dot{\varepsilon}_v^{\mathrm{p}} = \dot{\lambda}_m \frac{y^{*(m)}}{\partial \chi^v} \tag{80}$$

$$\dot{\varepsilon}_s^{\mathrm{p}} = \dot{\lambda}_m \frac{y^{*(m)}}{\partial \chi^s} \tag{81}$$

while the generic functions of erosion criterion and corresponding evolution rule are summarised as follows:

$$y^{(e)}\left(p^{'}, q, \frac{\partial p^w}{\partial x_i}, E\right) \leq 0 \tag{82}$$

$$\dot{E} = \dot{\lambda}_e \frac{y^{*(e)}}{\partial \chi^e} \tag{83}$$

From Eqs. (77) and (78), the incremental forms of stresses can be described as:

$$\dot{p}^{'} = \mu \frac{\partial^2 \psi^m}{\partial \varepsilon_v^2}\dot{\varepsilon}_v + \mu \frac{\partial^2 \psi^m}{\partial \varepsilon_v \partial \varepsilon_v^{\mathrm{p}}}\dot{\varepsilon}_v^{\mathrm{p}} + \frac{\partial \mu}{\partial E}\frac{\partial \psi^m}{\partial \varepsilon_v}\dot{E} \tag{84}$$

$$\dot{q} = \mu \frac{\partial^2 \psi^m}{\partial \varepsilon_s^2}\dot{\varepsilon}_s + \mu \frac{\partial^2 \psi^m}{\partial \varepsilon_s \partial \varepsilon_s^{\mathrm{p}}}\dot{\varepsilon}_s^{\mathrm{p}} + \frac{\partial \mu}{\partial E}\frac{\partial \psi^m}{\partial \varepsilon_s}\dot{E} \tag{85}$$

By substituting Eqs. (80) and (81) into Eqs. (84) and (85) and combining with Eq. (83), the incremental coupled hydro-mechanical-erosion relationships can be written in the following matrix form, given $\dot{\varepsilon}_v$, $\dot{\varepsilon}_s$ and $\frac{\partial \dot{p}^w}{\partial x_i}$ as inputs:

$$\begin{Bmatrix} \dot{p}^{'} \\ \dot{q} \\ \dot{E} \end{Bmatrix} = \begin{bmatrix} \mu\frac{\partial^2\psi^m}{\partial\varepsilon_v^2} & 0 & 0 \\ 0 & \mu\frac{\partial^2\psi^m}{\partial\varepsilon_s^2} & 0 \\ 0 & 0 & 0 \end{bmatrix} \begin{Bmatrix} \dot{\varepsilon}_v \\ \dot{\varepsilon}_s \\ \frac{\partial \dot{p}^w}{\partial x_i} \end{Bmatrix} + \begin{bmatrix} \mu\frac{\partial^2\psi^m}{\partial\varepsilon_v\partial\varepsilon_v^{\mathrm{p}}}\frac{y^{*(m)}}{\partial\chi^v} & \frac{\partial\mu}{\partial E}\frac{\partial\psi^m}{\partial\varepsilon_v}\frac{y^{*(e)}}{\partial\chi^e} \\ \mu\frac{\partial^2\psi^m}{\partial\varepsilon_s\partial\varepsilon_s^{\mathrm{p}}}\frac{y^{*(m)}}{\partial\chi^s} & \frac{\partial\mu}{\partial E}\frac{\partial\psi^m}{\partial\varepsilon_s}\frac{y^{*(e)}}{\partial\chi^e} \\ 0 & \frac{y^{*(e)}}{\partial\chi^e} \end{bmatrix} \begin{Bmatrix} \dot{\lambda}_m \\ \dot{\lambda}_e \end{Bmatrix} \tag{86}$$

Using yield functions in Eqs. (79) and (82), consistency conditions can be written as:

$$\dot{y}^{(m)} = \frac{\partial y^{(m)}}{\partial p^{'}}\dot{p}^{'} + \frac{\partial y^{(m)}}{\partial q}\dot{q} + \frac{\partial y^{(m)}}{\partial\left(\frac{\partial p^w}{\partial x_i}\right)}\frac{\partial \dot{p}^w}{\partial x_i} + \frac{\partial y^{(m)}}{\partial \varepsilon_v^{\mathrm{p}}}\dot{\varepsilon}_v^{\mathrm{p}} + \frac{\partial y^{(m)}}{\partial \varepsilon_s^{\mathrm{p}}}\dot{\varepsilon}_s^{\mathrm{p}} + \frac{\partial y^{(m)}}{\partial E}\dot{E} = 0 \tag{87}$$

$$\dot{y}^{(e)} = \frac{\partial y^{(e)}}{\partial p^{'}}\dot{p}^{'} + \frac{\partial y^{(e)}}{\partial q}\dot{q} + \frac{\partial y^{(e)}}{\partial\left(\frac{\partial p^w}{\partial x_i}\right)}\frac{\partial \dot{p}^w}{\partial x_i} + \frac{\partial y^{(e)}}{\partial E}\dot{E} = 0 \tag{88}$$

Substituting Eqs. (80) and (81), (83) and Eqs. (84) and (85) into Eqs. (87) and (88) leads to:

$$\begin{aligned} \dot{y}^{(m)} = {} & \frac{\partial y^{(m)}}{\partial p^{'}}\mu\frac{\partial^2\psi^m}{\partial\varepsilon_v^2}\dot{\varepsilon}_v + \frac{\partial y^{(m)}}{\partial q}\mu\frac{\partial^2\psi^m}{\partial\varepsilon_s^2}\dot{\varepsilon}_s + \frac{\partial y^{(m)}}{\partial\left(\frac{\partial p^w}{\partial x_i}\right)}\frac{\partial \dot{p}^w}{\partial x_i} + \left[\left(\frac{\partial y^{(m)}}{\partial p^{'}}\mu\frac{\partial^2\psi^m}{\partial\varepsilon_v\partial\varepsilon_v^{\mathrm{p}}} + \frac{\partial y^{(m)}}{\partial\varepsilon_v^{\mathrm{p}}}\right)\frac{y^{*(m)}}{\partial\chi^v} + \left(\frac{\partial y^{(m)}}{\partial q}\mu\frac{\partial^2\psi^m}{\partial\varepsilon_s\partial\varepsilon_s^{\mathrm{p}}} + \frac{\partial y^{(m)}}{\partial\varepsilon_s^{\mathrm{p}}}\right)\frac{y^{*(m)}}{\partial\chi^s}\right]\dot{\lambda}_m + \left(\frac{\partial y^{(m)}}{\partial p^{'}}\frac{\partial\mu}{\partial E}\frac{\partial\psi^m}{\partial\varepsilon_v} + \frac{\partial y^{(m)}}{\partial q}\frac{\partial\mu}{\partial E}\frac{\partial\psi^m}{\partial\varepsilon_s} + \frac{\partial y^{(m)}}{\partial E}\right)\frac{y^{*(e)}}{\partial\chi^e}\dot{\lambda}_e \\ & = 0 \end{aligned} \tag{89}$$

and

$$\begin{aligned} \dot{y}^{(e)} = {} & \frac{\partial y^{(e)}}{\partial p^{'}}\mu\frac{\partial^2\psi^m}{\partial\varepsilon_v^2}\dot{\varepsilon}_v + \frac{\partial y^{(e)}}{\partial q}\mu\frac{\partial^2\psi^m}{\partial\varepsilon_s^2}\dot{\varepsilon}_s + \frac{\partial y^{(e)}}{\partial\left(\frac{\partial p^w}{\partial x_i}\right)}\frac{\partial \dot{p}^w}{\partial x_i} \\ & + \left(\frac{\partial y^{(e)}}{\partial p^{'}}\mu\frac{\partial^2\psi^m}{\partial\varepsilon_v\partial\varepsilon_v^{\mathrm{p}}}\frac{y^{*(m)}}{\partial\chi^v} + \frac{\partial y^{(e)}}{\partial q}\mu\frac{\partial^2\psi^m}{\partial\varepsilon_s\partial\varepsilon_s^{\mathrm{p}}}\frac{y^{*(m)}}{\partial\chi^s}\right)\dot{\lambda}_m \\ & + \left(\frac{\partial y^{(e)}}{\partial p^{'}}\frac{\partial\mu}{\partial E}\frac{\partial\psi^m}{\partial\varepsilon_v} + \frac{\partial y^{(e)}}{\partial q}\frac{\partial\mu}{\partial E}\frac{\partial\psi^m}{\partial\varepsilon_s} + \frac{\partial y^{(e)}}{\partial E}\right)\frac{y^{*(e)}}{\partial\chi^e}\dot{\lambda}_e = 0 \end{aligned} \tag{90}$$

multipliers $\dot{\lambda}_m$ and $\dot{\lambda}_e$ can be obtained from Eqs. (89) and (90) in the following matrix form:

$$\begin{Bmatrix} \dot{\lambda}_m \\ \dot{\lambda}_e \end{Bmatrix} = -\begin{bmatrix} \Pi & \Lambda \\ \Omega & \mathrm{Y} \end{bmatrix}^{-1} \begin{bmatrix} \frac{\partial y^{(m)}}{\partial p^{'}}\mu\frac{\partial^2\psi^m}{\partial\varepsilon_v^2} & \frac{\partial y^{(m)}}{\partial q}\mu\frac{\partial^2\psi^m}{\partial\varepsilon_s^2} & \frac{\partial y^{(m)}}{\partial\left(\frac{\partial p^w}{\partial x_i}\right)} \\ \frac{\partial y^{(e)}}{\partial p^{'}}\mu\frac{\partial^2\psi^m}{\partial\varepsilon_v^2} & \frac{\partial y^{(e)}}{\partial q}\mu\frac{\partial^2\psi^m}{\partial\varepsilon_s^2} & \frac{\partial y^{(e)}}{\partial\left(\frac{\partial p^w}{\partial x_i}\right)} \end{bmatrix} \begin{Bmatrix} \dot{\varepsilon}_v \\ \dot{\varepsilon}_s \\ \frac{\partial \dot{p}^w}{\partial x_i} \end{Bmatrix} \tag{91}$$

where,

$$\Pi = \left(\frac{\partial y^{(m)}}{\partial p^{'}}\mu\frac{\partial^2\psi^m}{\partial\varepsilon_v\partial\varepsilon_v^{\mathrm{p}}} + \frac{\partial y^{(m)}}{\partial\varepsilon_v^{\mathrm{p}}}\right)\frac{y^{*(m)}}{\partial\chi^v} + \left(\frac{\partial y^{(m)}}{\partial q}\mu\frac{\partial^2\psi^m}{\partial\varepsilon_s\partial\varepsilon_s^{\mathrm{p}}} + \frac{\partial y^{(m)}}{\partial\varepsilon_s^{\mathrm{p}}}\right)\frac{y^{*(m)}}{\partial\chi^s} \tag{92}$$

$$\Lambda = \left(\frac{\partial y^{(m)}}{\partial p^{'}}\frac{\partial\mu}{\partial E}\frac{\partial\psi^m}{\partial\varepsilon_v} + \frac{\partial y^{(m)}}{\partial q}\frac{\partial\mu}{\partial E}\frac{\partial\psi^m}{\partial\varepsilon_s} + \frac{\partial y^{(m)}}{\partial E}\right)\frac{y^{*(e)}}{\partial\chi^e} \tag{93}$$

$$\Omega = \frac{\partial y^{(e)}}{\partial p^{'}}\mu\frac{\partial^2\psi^m}{\partial\varepsilon_v\partial\varepsilon_v^{\mathrm{p}}}\frac{y^{*(m)}}{\partial\chi^v} + \frac{\partial y^{(e)}}{\partial q}\mu\frac{\partial^2\psi^m}{\partial\varepsilon_s\partial\varepsilon_s^{\mathrm{p}}}\frac{y^{*(m)}}{\partial\chi^s} \tag{94}$$

$$\Upsilon = \left(\frac{\partial y^{(e)}}{\partial p^{'}}\frac{\partial \mu}{\partial E}\frac{\partial \psi^{m}}{\partial \varepsilon_{\nu}} + \frac{\partial y^{(e)}}{\partial q}\frac{\partial \mu}{\partial E}\frac{\partial \psi^{m}}{\partial \varepsilon_{s}} + \frac{\partial y^{(e)}}{\partial E}\right)\frac{y^{*(e)}}{\partial \chi^{e}} \tag{95}$$

Substituting Eq. (91) into Eq. (86), the expression of constitutive relationship can be presented as follows:

$$\begin{Bmatrix} \dot{p}^{'} \\ \dot{q} \\ \dot{E} \end{Bmatrix} = \begin{bmatrix} D^{\nu\nu} & D^{\nu s} & D^{\nu e} \\ D^{s\nu} & D^{ss} & D^{se} \\ D^{e\nu} & D^{es} & D^{ee} \end{bmatrix} \begin{Bmatrix} \dot{\varepsilon}_{\nu} \\ \dot{\varepsilon}_{s} \\ \dfrac{\partial \dot{p}^{w}}{\partial x_i} \end{Bmatrix}$$

$$= \left[\begin{bmatrix} \mu\dfrac{\partial^2\psi^m}{\partial\varepsilon_\nu^2} & 0 & 0 \\ 0 & \mu\dfrac{\partial^2\psi^m}{\partial\varepsilon_s^2} & 0 \\ 0 & 0 & 0 \end{bmatrix} - \begin{bmatrix} \mu\dfrac{\partial^2\psi^m}{\partial\varepsilon_\nu\partial\varepsilon_\nu^{\mathrm{p}}}\dfrac{y^{*(m)}}{\partial\chi^{\nu}} & \dfrac{\partial\mu}{\partial E}\dfrac{\partial\psi^m}{\partial\varepsilon_\nu}\dfrac{y^{*(e)}}{\partial\chi^e} \\ \mu\dfrac{\partial^2\psi^m}{\partial\varepsilon_s\partial\varepsilon_s^{\mathrm{p}}}\dfrac{y^{*(m)}}{\partial\chi^{s}} & \dfrac{\partial\mu}{\partial E}\dfrac{\partial\psi^m}{\partial\varepsilon_s}\dfrac{y^{*(e)}}{\partial\chi^e} \\ 0 & \dfrac{y^{*(e)}}{\partial\chi^e} \end{bmatrix} \begin{bmatrix} \Pi & \Lambda \\ \Omega & \Upsilon \end{bmatrix}^{-1} \begin{bmatrix} \dfrac{\partial y^{(m)}}{\partial p^{'}}\mu\dfrac{\partial^2\psi^m}{\partial\varepsilon_\nu^2} & \dfrac{\partial y^{(m)}}{\partial q}\mu\dfrac{\partial^2\psi^m}{\partial\varepsilon_s^2} & \dfrac{\partial y^{(m)}}{\partial\left(\frac{\partial p^w}{\partial x_i}\right)} \\ \dfrac{\partial y^{(e)}}{\partial p^{'}}\mu\dfrac{\partial^2\psi^m}{\partial\varepsilon_\nu^2} & \dfrac{\partial y^{(e)}}{\partial q}\mu\dfrac{\partial^2\psi^m}{\partial\varepsilon_s^2} & \dfrac{\partial y^{(e)}}{\partial\left(\frac{\partial p^w}{\partial x_i}\right)} \end{bmatrix}\right] \begin{Bmatrix} \dot{\varepsilon}_{\nu} \\ \dot{\varepsilon}_{s} \\ \dfrac{\partial \dot{p}^{w}}{\partial x_i} \end{Bmatrix} \tag{96}$$

where $D^{\nu\nu}$, $D^{\nu s}$, $D^{\nu e}$, $D^{s\nu}$, D^{ss}, D^{se}, $D^{e\nu}$, D^{es} and D^{ee} are terms of the tangent stiffnes written in the form of effective stress ($p^{'}$, q).

It can be seen in Eq. (96) that the inter-dependence between mechanical, hydraulic and erosion responses are reflected through the cross-coupling terms, leading to the path-dependent erosion law governed by hydro-mechanical loading paths. As a result, different responses under different hydraulic and mechanical loading conditions are induced by this path-dependence nature of both mechanical, seepage and erosion responses. This allows the current generic model to capture the grain-scale coupling between seepage flow, fine removals and grain rearrangements during processes of erosion and deformation.

We can rewrite the above incremental constitutive relationship of mean effective stress $p^{'}$ in an alternative form of Terzaghi stress ($\overline{p}$ with $\overline{p} = p - p^{w}$) by using the incremental form of effective stress presented in Eq. (46) ($p^{'} = \phi\overline{p} = \left[1 - \frac{(1-\alpha)\beta n^{es}}{(\beta n^{es} + n^{wf})[n^{s} + (1-\alpha)n^{es}]}\right]\overline{p}$ with $\phi = 1 - \frac{(1-\alpha)\beta n^{es}}{(\beta n^{es} + n^{wf})[n^{s} + (1-\alpha)n^{es}]}$) as follows:

$$\dot{\overline{p}} = \frac{1}{\phi}\dot{p}^{'} - \frac{1}{\phi}\overline{p}\left(\frac{\partial\phi}{\partial n^{es}}\dot{n}^{es} + \frac{\partial\phi}{\partial n^{s}}\dot{n}^{s} + \frac{\partial\phi}{\partial n^{wf}}\dot{n}^{wf}\right) \tag{97}$$

In the above expression, $\dot{n}^{es}$, $\dot{n}^{s}$ and $\dot{n}^{wf}$ can be replaced with the following expressions derived from Eqs. (19) to (22) and Eq. (39), using $\dot{\rho}_{ex} = \rho_{ex}^{u}\dot{E}$ and $\frac{\partial v_i^s}{\partial x_i} = -\dot{\varepsilon}_{\nu}$:

$$\dot{n}^{s} = n^{s}\dot{\varepsilon}_{\nu} - \frac{\rho_{ex}^{u}}{\rho^{s}}\dot{E} \tag{98}$$

$$\dot{n}^{es} = n^{es}\left(1 - \frac{\beta}{n^{wf} + n^{es}\beta}\right)\dot{\varepsilon}_{\nu} \tag{99}$$

$$\dot{n}^{wf} = -n^{wf}\frac{[n^{s} + n^{es}(1-\beta)]}{n^{wf} + n^{es}\beta}\dot{\varepsilon}_{\nu} + \frac{\rho_{ex}^{u}}{\rho^{s}}\dot{E} \tag{100}$$

Consequently, Eq. (97) can be rewritten as follows:

$$\dot{\overline{p}} = \frac{1}{\phi}\dot{p}^{'} + \frac{\overline{p}}{\phi}\left\{n^{wf}\frac{\partial\phi}{\partial n^{wf}}\frac{[n^{s} + n^{es}(1-\beta)]}{n^{wf} + n^{es}\beta} - n^{es}\frac{\partial\phi}{\partial n^{es}}\left(1 - \frac{\beta}{n^{wf} + n^{es}\beta}\right) - n^{s}\frac{\partial\phi}{\partial n^{s}}\right\}\dot{\varepsilon}_{\nu} + \frac{\overline{p}}{\phi}\left(\frac{\partial\phi}{\partial n^{s}}\frac{\rho_{ex}^{u}}{\rho^{s}} - \frac{\partial\phi}{\partial n^{wf}}\frac{\rho_{ex}^{u}}{\rho^{s}}\right)\dot{E} \tag{101}$$

Substituting $\dot{p}^{'} = D^{\nu\nu}\dot{\varepsilon}_{\nu} + D^{\nu s}\dot{\varepsilon}_{s} + D^{\nu e}\frac{\partial\dot{p}^{w}}{\partial x_i}$ and $\dot{E} = D^{e\nu}\dot{\varepsilon}_{\nu} + D^{es}\dot{\varepsilon}_{s} + D^{ee}\frac{\partial\dot{p}^{w}}{\partial x_i}$ as obtained from Eq. (96) into Eq. (101) results in:

$$\dot{\overline{p}} = \frac{\overline{p}}{\phi}\left\{\frac{D^{\nu\nu}}{\overline{p}} + n^{wf}\frac{\partial\phi}{\partial n^{wf}}\frac{[n^{s} + n^{es}(1-\beta)]}{n^{wf} + n^{es}\beta} + D^{e\nu}\left(\frac{\partial\phi}{\partial n^{s}}\frac{\rho_{ex}^{u}}{\rho^{s}} - \frac{\partial\phi}{\partial n^{wf}}\frac{\rho_{ex}^{u}}{\rho^{s}}\right) - n^{es}\frac{\partial\phi}{\partial n^{es}}\left(1 - \frac{\beta}{n^{wf} + n^{es}\beta}\right) - n^{s}\frac{\partial\phi}{\partial n^{s}}\right\}\dot{\varepsilon}_{\nu} + \frac{\overline{p}}{\phi}\left[\frac{D^{\nu s}}{\overline{p}} + D^{es}\left(\frac{\partial\phi}{\partial n^{s}}\frac{\rho_{ex}^{u}}{\rho^{s}} - \frac{\partial\phi}{\partial n^{wf}}\frac{\rho_{ex}^{u}}{\rho^{s}}\right)\right]\dot{\varepsilon}_{s} + \frac{\overline{p}}{\phi}\left[\frac{D^{\nu e}}{\overline{p}} + D^{ee}\left(\frac{\partial\phi}{\partial n^{s}}\frac{\rho_{ex}^{u}}{\rho^{s}} - \frac{\partial\phi}{\partial n^{wf}}\frac{\rho_{ex}^{u}}{\rho^{s}}\right)\right]\frac{\partial\dot{p}^{w}}{\partial x_i} \tag{102}$$

As can be seen in Eq. (102), α, β and n^{es} appear explicitly in tangent-stiffness terms for computing the increment of Terzaghi stress $\overline{p}$, indicating significant effects of the transition phase and erosion processes on behaviour of soils.

It is acknowledged that lack of data from both experiments and numerical simulations is the key challenge for the development and calibration of models derived from the proposed approach. Nevertheless, this key challenge in our opinion is a consequence of the lack of a theoretical framework that can appropriately describe internal erosion processes and their effects on both mechanical and hydraulic responses of soils at the continuum scale. The proposed theoretical approach in this study fits into that gap, in providing work conjugate quantities along with expression of effective stress with the influence of internal erosion. These findings can help direct the design of both numerical and physical experiments, along with the quantification of the produced data so that findings from can be useful for constitutive modelling. Based on the proposed form of work, we can quantify how much hydraulic and mechanical energy is produced or dissipated within the total budget of energy. This allows the formulation of seepage (see Eq. (68)), mechanical ((see Eqs. (71) to (73))) and erosion (see Eqs. (75) and (76)) criteria, leading to tangent stiffness matrix with the cross-coupling terms in Eqs. (96) and (102).

The above features reflect the promising capacity of our formulation in capturing the coupling between erosion, hydraulic and mechanical processes. This coupling is implicitly reflected in the mutual solid-fluid transformations and interactions governed by four main factors: soil susceptibility, stress condition, loading path, and hydraulic gradient as investigated in several experiments (Chang and Zhang, 2013; Hunter

and Bowman, 2018; Prasomsri and Takahashi, 2020; Sato and Kuwano, 2018; Nguyen et al., 2018; Nguyen et al., 2019).

5. Conclusions

In this study, we develop a formulation of work input to reflect underlying mechanisms of internal erosion in fully saturated soils. The basis of the formulation development is the intrinsic nature of the mutual transition and interaction between grain and fluid at the grain contacts, which governs the simultaneous processes of deformation, seepage velocity and mass loss at the continuum level. For this purpose, a transition phase containing grains potentially to be eroded is needed to describe the sudden transition in stress and velocity of the erodible solid and their influence on effective stress of the soil skeleton. This mechanism is integrated into a thermodynamics-based approach taking into account mass exchanges and momentum conservation equations of different phases, in conjunction with their interaction. This automatically leads to three work conjugate pairs governing mechanical (effective stress-strain), erosion (erosion force-mass loss) and seepage (hydraulic gradient-water flux) responses within a new form of work input (see Eq. (45)) to reflect the effect of erosion on hydromechanical coupling.

The proposed approach also leads to a new form of effective stress (see Eq. (46)) being able to account for the effect of mass loss due to erosion on soil skeleton stress. The work-conjugate pairs obtained allows an appropriate selection of variables and their interactions which is important for the development of constitutive models for soils undergoing internal erosion. This is demonstrated through an example of a generic thermodynamics-based constitutive model with seepage (see Eq. (68)), mechanical ((see Eqs. (71) to (73))) and erosion (see Eqs. (75) and (76)) criteria as presented in Section 4.3. Its hydromechanical tangent stiffness with cross-coupling terms (see Eqs. (96) and (102)) shows the inter-dependence between mechanical, hydraulic and erosion responses. The thermodynamic formulation and model are presented in generic forms and further work is needed to explore the potentials of the proposed framework.

Declaration of Competing Interest

The authors declare that they have no known competing financial interests or personal relationships that could have appeared to influence the work reported in this paper.

Data availability

No data was used for the research described in the article.

Acknowledgements

The authors gratefully acknowledge support from the Australian Research Council via Discovery Projects DP190102779 (Bui & Nguyen), and FT200100884 (Bui).

References

Aichi, M., Tokunaga, T., 2012. Material coefficients of multiphase thermoporoelasticity for anisotropic micro-heterogeneous porous media. International Journal of Solids and Structures 49 (23–24), 3388–3396.
Andrade, J.E., et al., 2012. On the rheology of dilative granular media: bridging solid-and fluid-like behavior. Journal of the Mechanics and Physics of Solids 60, 1122–1136.
Andrade, J.E., et al., 2022. Measuring Terzaghi's effective stress by decoding force transmission in fluid-saturated granular media. Journal of the Mechanics and Physics of Solids 104912.
Benallal, A., Claudia, C., 2003. Perturbation growth and localization in fluid-saturated inelastic porous media under quasi-static loadings. Journal of the Mechanics and Physics of Solids 51, 851–899.
Bendahmane, F., Marot, D., Alexis, A., 2008. Experimental parametric study of suffusion and backward erosion. Journal of geotechnical and geoenvironmental engineering 134 (1), 57–67.
Biot M.A. (1941). "General theory of three-dimensional consolidation." Journal of applied physics. **12**(2). 155-164.
Bonelli, S., Marot, D., 2011. Micromechanical modeling of internal erosion. European Journal of Environmental and Civil Engineering 15 (8), 1207–1224.
Borja, R.I., et al., 2013. Shear band in sand with spatially varying density. Journal of the Mechanics and Physics of Solids 61, 219–234.
R.I. Borja, J.A. White. (2010). Conservation laws for coupled hydro-mechanical processes in unsaturated porous media: theory and implementation, Lawrence Livermore National Lab.(LLNL), Livermore, CA (United States).
Borja, R.I., Koliji, A., 2009. On the effective stress in unsaturated porous continua with double porosity. Journal of the Mechanics and Physics of Solids 57 (8), 1182–1193.
Bui, H.H., Nguyen, G.D., 2017. A coupled fluid-solid SPH approach to modelling flow through deformable porous media. International Journal of Solids and Structures 125, 244–264.
Chang, D., Zhang, L.M., 2011. A stress-controlled erosion apparatus for studying internal erosion in soils. Geotechnical Testing Journal 34 (6), 579–589.
Chang, D.S., Zhang, L.M., 2013. Extended internal stability criteria for soils under seepage. Soils and Foundations 53 (4), 569–583.
Chen, X., et al., 2021. Theory of fluid saturated porouse media with surface effects. Journal of the Mechanics and Physics of Solids 151, 104392.
Cheng, K., et al., 2021. Un-resolved CFD-DEM method: An insight into its limitations in the modelling of suffusion in gap-graded soils. Powder Technology 381, 520–538.
Cividini, A., Bonomi, S., Vignati, G.C., Gioda, G., 2009. Seepage-induced erosion in granular soil and consequent settlements. International Journal of Geomechanics 9 (4), 187–194.
Coussy, O., 2006. Deformation and stress from in-pore drying-induced crystallization of salt. Journal of the Mechanics and Physics of Solids 54, 1517–1547.
Coussy, O., et al., 2010. Revisiting the thermodynamics of hardening plasticity for unsaturated soils. Computers and Geotechnics 37 (1–2), 207–215.
Das, A., et al., 2014. A thermomechanical constitutive model for cemented granular materials with quantifiable internal variables. Part II–validation and localization analysis. Journal of the Mechanics and Physics of Solids 70, 382–405.
Duriez, J., et al., 2017. The micromechanical nature of stresses in triphasic granular media with interfaces. Journal of the Mechanics and Physics of Solids 99, 495–511.
Einav, I., 2007a. Breakage mechanics—part I: theory. Journal of the Mechanics and Physics of Solids 55 (6), 1274–1297.
Einav, I., 2007b. Breakage mechanics—Part II: Modelling granular materials. Journal of the Mechanics and Physics of Solids 55 (6), 1298–1320.
Einav, I., Liu, M., 2018. Hydrodynamic derivation of the work input to fully and partially saturated soils. Journal of the Mechanics and Physics of Solids 110, 205–217.
Einav, I., Valdes, J.R., 2008. On comminution and yield in brittle granular mixtures. Journal of the Mechanics and Physics of Solids 56, 2136–2148.
El Tabbal, G., et al., 2020. Modelling the drying shrinkage of porous materials by considering both capillary and adsorption effects. Journal of the Mechanics and Physics of Solids 142, 104016.
Foster, M., Fell, R., Spannagle, M., 2000. The statistics of embankment dam failures and accidents. Canadian Geotechnical Journal 37 (5), 1000–1024.
Gajo, A., 2011. Finite strain hyperelastoplastic modelling of saturated porous media with compressible constituents. International Journal of Solids and Structures 48 (11–12), 1738–1753.
Gawin, D., Pesavento, F., Koniorczyk, M., Schrefler, B.A., 2020. Poro-mechanical model of strain hysteresis due to cyclic water freezing in partially saturated porous media. International Journal of Solids and Structures 206, 322–339.
Gray, W.G., Schrefler, B.A., Pesavento, F., 2009. The solid phase stress tensor in porous media mechanics and the Hill-Mandel condition. Journal of the Mechanics and Physics of Solids 57 (3), 539–554.
Gray, W.G., Schrefler, B.A., Pesavento, F., 2010. Work input for unsaturated elastic porous media. Journal of the Mechanics and Physics of Solids 58 (5), 752–765.
Gu, D.M., et al., 2019. A DEM-based approach for modeling the evolution process of seepage-induced erosion in clayey sand. Acta Geotechnica 14, 1629–1641.
Houlsby, G., 1979. The work input to a granular material. Géotechnique 29 (3), 354–358.
Houlsby, G., 1997. The work input to an unsaturated granular material. Géotechnique 47 (1), 193–196.
Houlsby, G., Puzrin, A., 2000. A thermomechanical framework for constitutive models for rate-independent dissipative materials. International journal of Plasticity 16 (9), 1017–1047.
Houlsby, G.T., Puzrin, A.M., 2007. Principles of hyperplasticity: an approach to plasticity theory based on thermodynamic principles. Springer Science & Business Media.
Hu, Z., et al., 2019. Suffusion-induced deformation and microstructural change of granular soils: a coupled CFD–DEM study. Acta Geotechnica 14, 795–814.
Hu, Z., et al., 2020. Suffusion-induced evolution of mechanical and microstructural properties of gap-graded soils using CFD-DEM. Journal of geotechnical and geoenvironmental engineering 146 (5), 04020024.
Hunter, R., Bowman, E., 2018. Visualisation of seepage-induced suffusion and suffosion within internally erodible granular media. Géotechnique 68 (10), 918–930.
Jiang, Y., et al., 2017. A thermodynamic treatment of partially saturated soils revealing the structure of effective stress. Journal of the Mechanics and Physics of Solids 100, 131–146.
Kuwano, R., et al., 2021. Change in mechanical behaviour of gap-graded soil subjected to internal erosion observed in triaxial compression and torsional shear. Geomechanics for Energy and the Environment 27, 100197.
Lemaitre, J., 2012. A Course on Damage Mechanics. Springer, Berlin, Heidelberg.
Liang, Y., Yeh, T.-C., Chen, Q., Xu, W., Dang, X., Hao, Y., 2019. Particle erosion in suffusion under isotropic and anisotropic stress states. Soils and Foundations 59 (5), 1371–1384.

Liu, Y., Wang, L., Hong, Y.i., Zhao, J., Yin, Z.-Y., 2020. A coupled CFD-DEM investigation of suffusion of gap graded soil: Coupling effect of confining pressure and fines content. International Journal for Numerical and Analytical Methods in Geomechanics 44 (18), 2473–2500.
Loret, B., Khalili, N., 2002. An effective stress elastic–plastic model for unsaturated porous media. Mechanics of Materials 34 (2), 97–116.
Loret, B., Rizzi, E., 1999. Strain localization in fluid-saturated anisotropic elastic–plastic porous media with double porosity. Journal of the Mechanics and Physics of Solids 47 (3), 503–530.
Ma, Q., et al., 2021. Microscopic mechanism of particle detachment in granular materials subjected to suffusion in anisotropic stress states. Acta Geotechnica 16, 2575–2591.
Madeo, A., et al., 2013. A continuum model for deformable, second gradient porous media partially saturated with compressible fluids. Journal of the Mechanics and Physics of Solids 61, 2196–2211.
Moffat, R.A., Fannin, R.J., 2006. A large permeameter for study of internal stability in cohesionless soils. Geotechnical Testing Journal 29 (4), 273–279.
Muir wood, D., Maeda, K., Nukudani, E., 2010. Modelling mechanical consequences of erosion. Géotechnique 60 (6), 447–457.
Nguyen, C.D., et al., 2019. Experimental investigation of microstructural changes in soils eroded by suffusion using X-ray tomography. Acta Geotechnica 14, 749–765.
Nguyen, G.D., Bui, H.H., 2020. A thermodynamics- and mechanism-based framework for constitutive models with evolving thickness of localisation band. International Journal of Solids and Structures 187 (100–120), 100–120.
Nguyen, D.G., Einav, I., 2010. Nonlocal regularisation of a model based on breakage mechanics for granular materials. International Journal of Solids and Structures 47 (10), 1350–1360.
Nguyen C., et al. (2018). The effect of suffusion on physical properties and mechanical behavior of granular soils. 9th International Conference of Scour and Erosion, ICSE, CRC Press.
Nie, Z., Fang, C., Gong, J., Yin, Z.-Y., 2020. Exploring the effect of particle shape caused by erosion on the shear behaviour of granular materials via the DEM. International Journal of Solids and Structures 202, 1–11.
Oka, F., Kimoto, S., Takada, N., Gotoh, H., Higo, Y., 2010. A seepage-deformation coupled analysis of an unsaturated river embankment using a multiphase elasto-viscoplastic theory. Soils and Foundations 50 (4), 483–494.
Phan, D.G., et al., 2021a. Constitutive modelling of partially saturated soils: Hydro-mechanical coupling in a generic thermodynamics-based formulatio. International Journal of Plasticity 136, 102821.
Phan, D.G., et al., 2023b. Capturing the transition from diffuse to localised failure in constitutive modelling of partially saturated soils. International Journal of Plasticity under revision.
Phan DG., et al (2021b). "A thermodynamics-based formulation for coupled hydro-mechanical behaviour of unsaturated soils", The 16th International Association for Computer Methods and Advances in Geomechanics, IACMAG 2021, Turin May 5th-8th.
Phan, D.G., Nguyen, G.D., Bui, H.H., Bennett, T., 2023a. The effect of hydro-mechanical coupling on the onset and orientation of localisation bands in partially saturated soils. International Journal of Plasticity 162, 103551.
Phan, DG. 2021 "A thermodynamic approach to modelling pre-and post-localisation behaviour of partially saturated soils for failure analysis using the Smoothed Particle Hydrodynamics", PhD Thesis, University of Adelaide.
Prasomsri, J., Takahashi, A., 2020. The role of fines on internal instability and its impact on undrained mechanical response of gap-graded soils. Soils and Foundations 60 (6), 1468–1488.
Radjai, F., et al., 1998. Bimodal character of stress transmission in granular packings. Physical review letters 80 (1), 61.
Ricken, T., et al., 2022. Theoretical formulation and computational aspects of a two-scale homogenization scheme combining the TPM and FE method for poro-elastic fluid-saturated porous media. International Journal of Solids and Structures 241, 111412.
Rousseau, Q., Sciarra, G., Gelet, R., Marot, D., 2020. Modelling the poroelastoplastic behaviour of soils subjected to internal erosion by suffusion. International Journal for Numerical and Analytical Methods in Geomechanics 44 (1), 117–136.
Sato, M., Kuwano, R., 2018. Laboratory testing for evaluation of the influence of a small degree of internal erosion on deformation and stiffness. Soils and Foundations 58 (3), 547–562.
Sciarra, G., 2016. Phase field modeling of partially saturated deformable porous media. Journal of the Mechanics and Physics of Solids 94, 230–256.
Selvadurai, A.P.S., Suvorov, A.P., 2016. Coupled hydro-mechanical effects in a poro-hyperelastic material. Journal of the Mechanics and Physics of Solids 91, 311–333.
Serpieri, R., Travascio, F., Asfour, S., Rosati, L., 2015. Variationally consistent derivation of the stress partitioning law in saturated porous media. International Journal of Solids and Structures 56-57, 235–247.
Shire, T., et al., 2014. Fabric and effective stress distribution in internally unstable soils. Journal of geotechnical and geoenvironmental engineering 140 (12), 04014072.
Shire, T., O'sullivan, C., 2013. Micromechanical assessment of an internal stability criterion. Acta Geotechnica 8, 81–90.
Song, X., Silling, S.A., 2020. On the peridynamic effective force state and multiphase constitutive correspondence principle. Journal of the Mechanics and Physics of Solids 145, 104161.
Steeb, H., Diebels, S., 2003. A thermodynamic-consistent model describing growth and remodeling phenomena. Computational materials science 28 (3–4), 597–607.
Tengattini, A., et al., 2014. A thermomechanical constitutive model for cemented granular materials with quantifiable internal variables. Part I—Theory. Journal of the Mechanics and Physics of Solids 70, 281–296.
Thornton, C., Antony, S., 1998. Quasi–static deformation of particulate media. Philosophical Transactions of the Royal Society of London. Series A: Mathematical, Physical and Engineering Sciences 356 (1747), 2763–2782.
Vernerey, F.J., 2011. A theoretical treatment on the mechanics of interfaces in deformable porous media. International Journal of Solids and Structures 48 (22–23), 3129–3141.
Wan, C.F., Fell, R., 2004. Investigation of rate of erosion of soils in embankment dams. Journal of geotechnical and geoenvironmental engineering 130 (4), 373–380.
Wan, C.F., Fell, R., 2008. Assessing the potential of internal instability and suffusion in embankment dams and their foundations. Journal of geotechnical and geoenvironmental engineering 134 (3), 401–407.
Wang, G., et al., 2020. Effects of internal erosion on parameters of subloading Cam-Clay model. Geotechnical and Geological Engineering 38, 1323–1335.
Yang, R., Lemarchand, E., Fen-Chong, T., Azouni, A., 2015. A micromechanics model for partial freezing in porous media. International Journal of Solids and Structures 75-76, 109–121.
Yang, J., Yin, Z.-Y., Laouafa, F., Hicher, P.-Y., 2019. Internal erosion in dike-on-foundation modeled by a coupled hydromechanical approach. International Journal for Numerical and Analytical Methods in Geomechanics 43 (3), 663–683.
Yin, Y., et al., 2021. Solid–fluid sequentially coupled simulation of internal erosion of soils due to seepage. Granular Matter 23 (2), 20.
Zhang, X., et al., 2013. A thermodynamics-based model on the internal erosion of earth structures. Geotechnical and Geological Engineering 31, 479–492.
Zhang, X., et al., 2015. Study of soil structures strength and stiffness loss based on thermodynamics and continuum mechanics. Environmental Earth Sciences 73, 4143–4149.
Zhou, G.G., et al., 2019. Experimental investigation on the longitudinal evolution of landslide dam breaching and outburst floods. Geomorphology 334, 29–43.
Zhou, W., et al., 2020. Microscopic investigation of internal erosion in binary mixtures via the coupled LBM-DEM method. Powder Technology 376, 31–41.
Ziegler, H., 2012. An introduction to thermomechanics. Elsevier.
Zienkiewicz, O.C., et al., 1990. Static and dynamic behaviour of soils: a rational approach to quantitative solutions. I. Fully saturated problems. Proceedings of the Royal Society of London. A. Mathematical and Physical Sciences 429 (1877), 285–309.
Zou, Y., et al., 2020. Simulating progression of internal erosion in gap-graded sandy gravels using coupled CFD-DEM. International Journal of Geomechanics 20 (1), 04019135.